AD NUMBER

AD815371

LIMITATION CHANGES

TO:

Approved for public release; distribution is unlimited.

FROM:

**Distribution authorized to U.S. Gov't. agencies and their contractors;
Administrative/Operational Use; MAY 1967. Other requests shall be referred to Air Force Avionics Lab., Wright-Patterson AFB, OH 45433.**

AUTHORITY

AFAL ltr 30 Jul 1973

ITR-1/F33615-67-C-1435

GASEOUS ION LASER RESEARCH

HUGHES RESEARCH LABORATORIES
MALIBU, CALIFORNIA

INTERIM TECHNICAL REPORT NO. 1

MAY 1967

AIR FORCE AVIONICS LABORATORY
RESEARCH AND TECHNOLOGY DIVISION
AIR FORCE SYSTEMS COMMAND
WRIGHT-PATTERSON AIR FORCE BASE, OHIO 4543[illegible]

GASEOUS ION LASER RESEARCH

Interim Technical Report No. 1
Contract No. F33615-67-C-1435

A. S. Halsted, W. B. Bridges, H. R. Friedrich
Hughes Research Laboratories
Malibu, California 90265

Sponsored by

Air Force Avionics Laboratory
Research and Technology Division
Air Force Systems Command
Wright-Patterson Air Force Base Ohio 45433

TABLE OF CONTENTS

LIST OF ILLUSTRATIONS

ABSTRACT

The general objectives of this contract are to extend the lifetime and reliability of high power ion lasers and to improve their operating characteristics. Specific tasks which will be undertaken during the program are outlined. A cathode evaluation program has been initiated; complete life test data on a hot oxide cathode are presented. The results of an evaluation of pyrolytic graphite and pyrolytic overcoated graphite segments are given. An improved design of radiation-cooled anode has been developed and tested. Preliminary studies of noise modulation of the output beam with particular emphasis on fluctuations introduced by power supply ripple are described.

I. INTRODUCTION

The objective of this program is to demonstrate the feasibility of building high power (>1 W) argon ion lasers which are suitable for field use and have a mean time between failure of more than 1000 hours. Attention is also being given to operational simplicity and output properties necessary for the laser to be useful in military systems.

The studies performed under this contract draw heavily upon the results of the previous 15-month Air Force contract (AF 33(615)-3077) of the same title. To provide a brief review of the scope of the previous work and to place the objectives of the present program in better perspective, the abstract of that contract's final report, AFAL-TR-67-89, is quoted below:

> "The basic mechanisms of ion lasers are discussed and scaling laws derived based on these mechanisms. The results of a parametric study confirming these scaling laws are presented. Measurements of power output and efficiency as a function of tube diameter, length, gas pressure, magnetic field, and mirror transmission are given and compared with theory. Plasma properties are summarized, including magnetic field effects and conditions in the bore constrictions. The design and performance characteristics of high power lasers constructed with quartz, ceramic, and segmented metal and graphite bores are reported. A theory for gas pumping in low pressure arcs is presented and compared with the measured rates of gas pumping in ion lasers. The dependence of the gas pumping rate on gas pressure, discharge current, magnetic field, and external gas return path is given. Problems with mirror damage and mode distortion in high power argon lasers are described. Based on the results of a mirror evaluation program, mirrors and surface cleaning techniques are recommended."

Briefly, the present state of the art in ion laser development is that scaling laws which predict the tradeoffs among power output, size, and efficiency are well understood, and all of the problem areas associated with ion laser construction have been clearly identified. The remaining task is to achieve long tube life and operational simplicity.

The technical effort of this program to achieve these objectives may be divided into three activities:

1. life testing of critical discharge tube elements (cathode, bore, tube envelope) to determine the failure modes for the most practical materials and configurations;

2. evaluation of bore, throat, and vacuum envelope designs to minimize erosion and/or localized damage;

3. measurement and improvement of operational characteristics which are critical to applications in military systems.

A chart indicating the particular tasks to be undertaken and the approximate time sequence of the contract effort is shown in Fig. 1.

In Section II of this report, general considerations affecting the choice of cathodes for use in ion lasers are discussed. A successful 1700 hour life test of a hot oxide cathode completed during the past quarter is described.

Section III describes bore material studies. Under the previous contract, quartz, alumina, molybdenum, tungsten, and graphite were evaluated as bore materials. During the past quarter we have evaluated pyrolytic graphite and normal graphite with an overcoating of pyrolytic graphite as bore materials. Each material was tested for more than 200 hours. The properties of these materials, their performance in the laser (cleanliness, gas cleanup rate, etc), and resistance to erosion are described in detail.

The design and performance of a radiation-cooled anode is described in Section IV. Initial studies of noise on the output beam, with particular emphasis on fluctuations introduced by anode, filament, and solenoid supplies, are described in Section V.

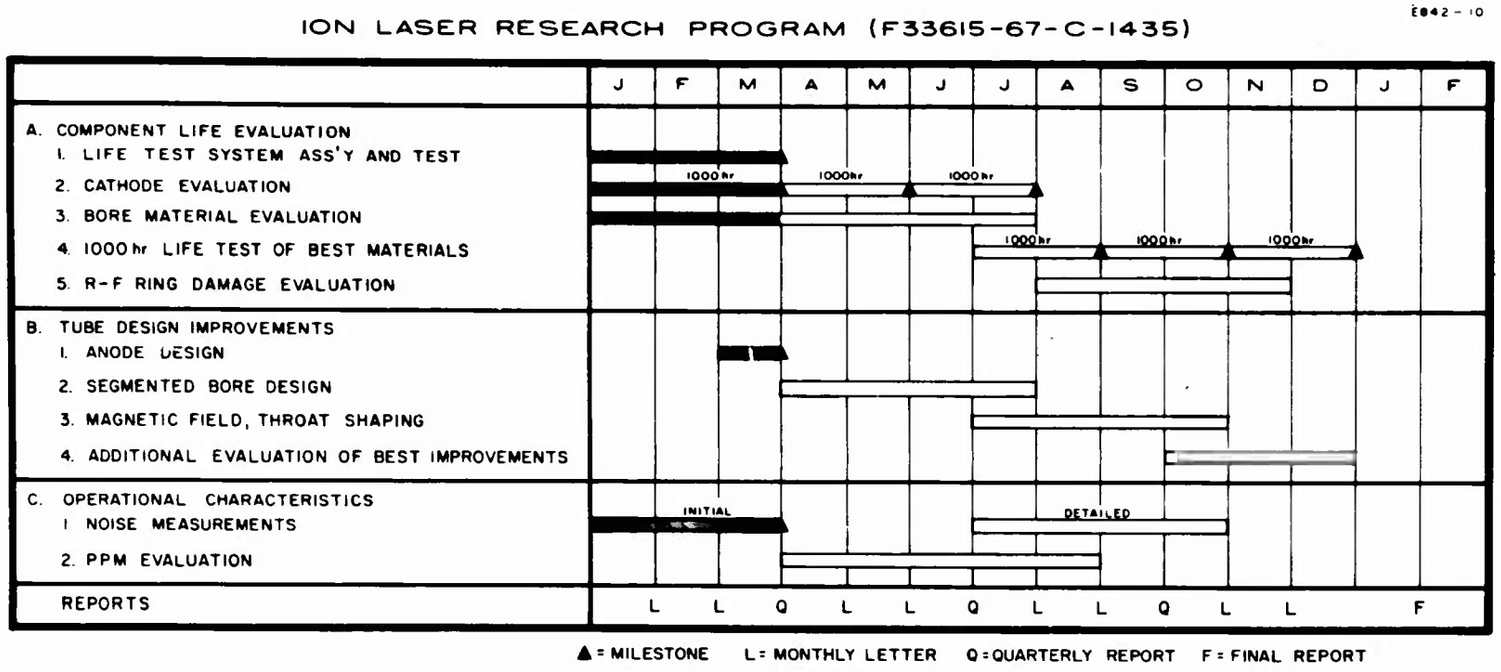

Fig. 1. Ion laser research program schedule.

II. CATHODE EVALUATION

The objective of this effort is the measurement of the operating characteristics of cathodes which are suitable for use in ion lasers. The operating characteristics of interest are the lifetime, efficiency, current capability, gas cleanup rate, and resistance to poisoning.

A. Selection of Cathode Type

The basic equation for the rate of thermal emission of electrons from a heated solid is given by the Richardson-Dushman equation

$$J = AT^2 \exp(-\phi/kT) \qquad (1)$$

where J is the thermionic emission in amperes per square centimeter A is a fundamental constant equal to 120 $A/cm^2\text{-}^oK^2$, k is the Boltzmann constant, T is the temperature (^oK), and ϕ is the potential barrier that the electrons must overcome to go from the Fermi level inside to the vacuum level outside of the solid. Emission properties of a surface depend critically on ϕ; typical values of ϕ are 1.5 eV for oxide cathodes, 2.0 eV for tungsten matrix cathodes, 2.6 to 3.2 eV for refractory coated cathodes (Gd_2O_3, LaB_6, ThO_2), 3.1 eV for thoriated tungsten, and 3.4 to 5 eV for metal cathodes. Figure 2 shows the emission characteristics of thermionic cathode types which are capable of emitting a sufficiently high current density (>1 A/cm^2) to be of interest for ion laser use.[1]

The major advantage of oxide cathodes is, of course, the low operating temperature, and therefore low heater power, required per emitted ampere. We have used this type of laser exclusively in our ion laser program. A successful 1700 hour life test of this type of cathode was completed during this quarter.

Nickel matrix cathodes, the second most efficient type, act essentially as patchy oxide cathodes and have no particular advantage over oxide cathodes unless intricate shapes are required.[1]

Many different types of tungsten matrix cathodes (L cathodes, impregnated cathodes, dispenser cathodes, etc.) have been discussed in the literature. In all of these cathode types, barium diffuses through porous tungsten to form an emitting layer on the tungsten surface. The higher operating temperature of this cathode makes it inherently less efficient than the oxide cathode at a given current density; for an emission

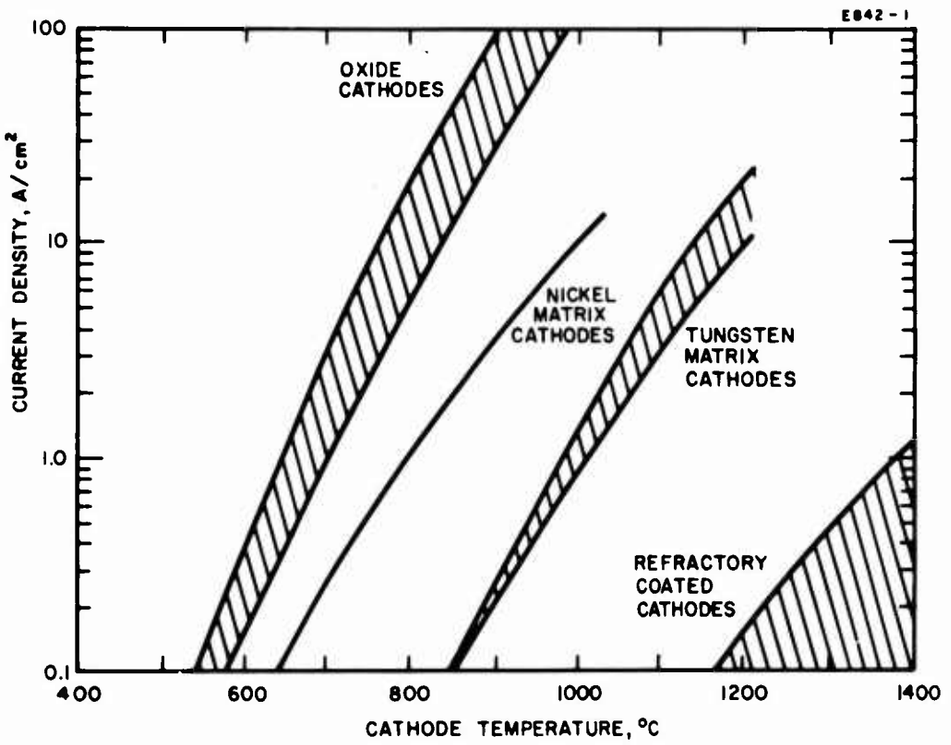

Fig. 2. Emission current density versus surface temperature for different cathode types.

current of 1A/cm^2, the oxide cathode requires one fifth the heater power. The advantages of tungsten matrix cathodes are (1) mechanical ruggedness and (2) ability to supply continuously high current densities (5 to 10 A/cm^2). Hernqvist and Fendley[2] have recently reported >1000 hours of life at 9 A for this type of cathode. Other indications are that these cathodes are easily damaged by ion sputtering in high power lasers, however.[3]

We have purchased several impregnated tungsten cathodes from Spectromat, Inc. These cathodes will be evaluated during the next quarter and their performance compared with that of oxide cathodes.

B. Description of the Hughes Ion Laser Oxide Cathode

The cathodes used in our laser program are directly heated, oxide-coated nickel mesh structures such as that shown in Fig. 3. The completed cathode has a triple heat shield with a 1/2 in. diameter hole in the front for electron extraction. Another hole in the rear allows passage of the laser beam so that the cathodes may be mounted coaxially with the beam.

These cathodes were developed specifically for ion lasers and were initially fabricated at the Research Laboratories. They are now built as a product by the Hughes Electron Dynamics Division (EDD). The flower-shaped mesh shown in Fig. 3 has an area of 24 cm^2 and is coated with the two-carbonate coating used at EDD for space-qualified TWT's; in this application the cathode is maintained at 725°C and emits 250 mA/cm^2 for >20,000 hours.

In ion laser applications, which require high current densities, the cathode temperature is maintained at 850°C. The input power to the cathode to maintain this temperature is approximately 60 W (25 A at 2.4 V).

Evaporation of the oxide coating starts to occur above 800°C. Evaporation and/or ion sputtering of the oxide coating should be the life-limiting cathode processes.

C. Prior Experience with the Hughes Oxide Cathode

Roughly 90 ion lasers (experimental and production tubes) have been built using this type of oxide cathode. The maximum values of discharge currents which have been drawn are 50 A dc (in a 10 W cw laser) and 450 A pulsed (in a 50 W peak power laser). No life test data have been taken under these extreme conditions; we know the life is >50 hours at 50 A dc, however. Lifetimes at 20 A of >200 hours, and in one case >600 hours, have been reported for 2 W quartz-bore lasers operating in the field. Tube failure, when it has occurred, has been for other reasons.

M 3690

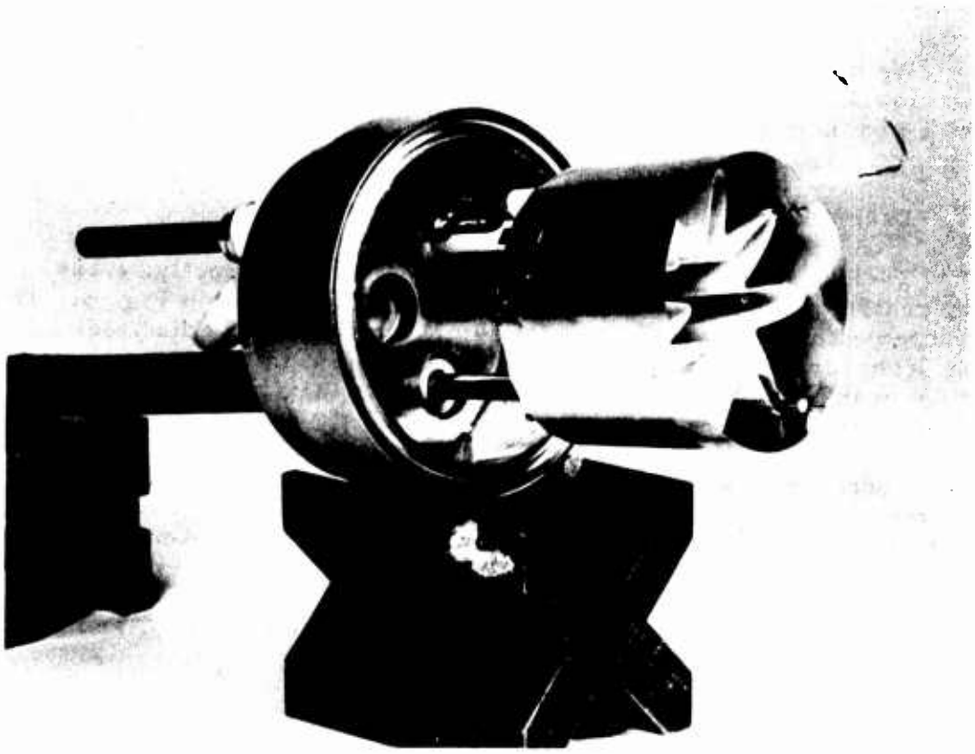

Fig. 3. Hughes ion laser oxide cathode.

We find oxide cathodes to be very resistant to poisoning in argon lasers. It is not necessary to bake out tubes under vacuum before striking the discharge. Instead, our standard procedure is to clean up the tube by running the discharge for short periods and then pumping out and refilling the tube; five to ten such refills are usually adequate. The cathodes may be let down to argon, helium, or dry nitrogen atmosphere repeatedly for minor tube repairs (such as window replacement) without impairing their operation. This is in agreement with the results of Haas and Jensen,[4] who have shown that cathode poisoning is largely caused by the absorption of water vapor, and that good emission will be maintained if the cathode is kept at 150°C during exposure to air.

D. Cathode Test Apparatus

The experimental apparatus used to evaluate cathode performance is shown in Fig. 4. Figure 5 is a schematic representation. The cathode and water-cooled anode are separated by a 1-1/2 in. diameter, 5 in. long quartz bore. This configuration reproduces the electrodes and approach arms, but not the bore or constrictions, of quartz and segmented bore tubes. A thermocouple gauge, getter, gas leak valve, and high pressure argon reservoir are located on a side arm. The Hasting thermocouple gauge was calibrated for argon using a McLeod gauge. The volume of the tube is 0.7 ℓ.

E. Experimental Results

An oxide cathode was operated for 1700 hours before being disassembled for inspection. The discharge current was 20 A for the first 1100 hours, and was varied between 10 and 20 A during the last 600 hours to determine the dependence of gas cleanup rate (GCR) on current. Particular attention was paid to the GCR throughout the run since we wished to determine what fraction of the GCR measured in bore material experiments is attributable to the bore material and what part to the cathode and anode.

Experimental results are shown in Figs. 6, 7, and 8. Figure 6 shows the variation in gas pressure during operation at 20 A. The tube was operated in 8-hour and then 23-hour increments. The gas pressure was recorded both while the discharge was on (solid line), and when the tube was shut off; this provided a measurement under uniform, cold conditions. When the cold filling pressure fell to 0.1 Torr, gas was added to obtain a pressure of 0.28 Torr, and the test continued.

It is clear from Fig. 6 that there is a continual aging process going on with each successive run exhibiting a lower gas clean up rate. The average GCR was 3.5 $\mu\ell$/hour for the first run (10 to 40 hours) and 0.46 $\mu\ell$/hour for the last complete run (790 to 1066 hours). This

M 5428

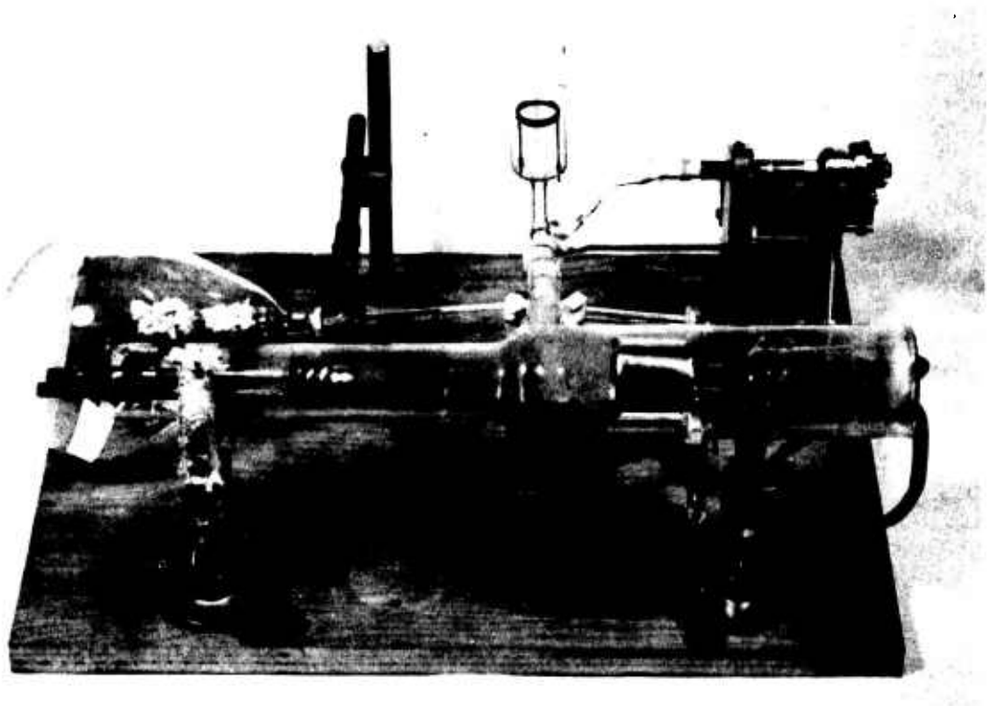

Fig. 4. Photograph of cathode evaluation apparatus.

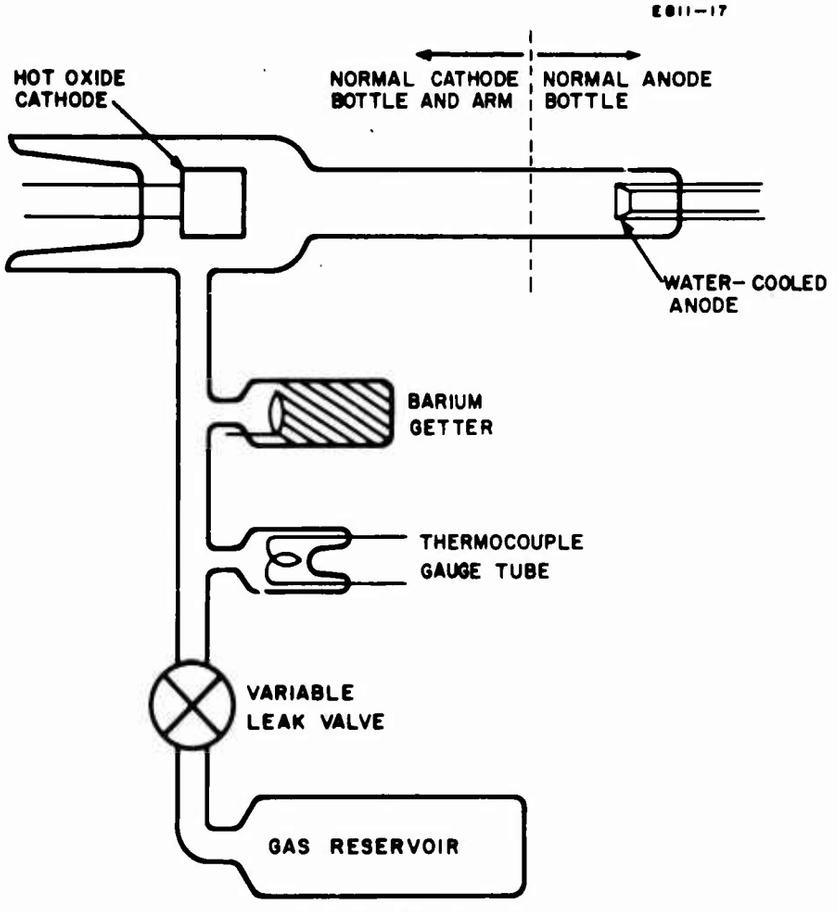

Fig. 5. Schematic representation of experimental apparatus used to monitor the gas cleanup rate of a laser cathode.

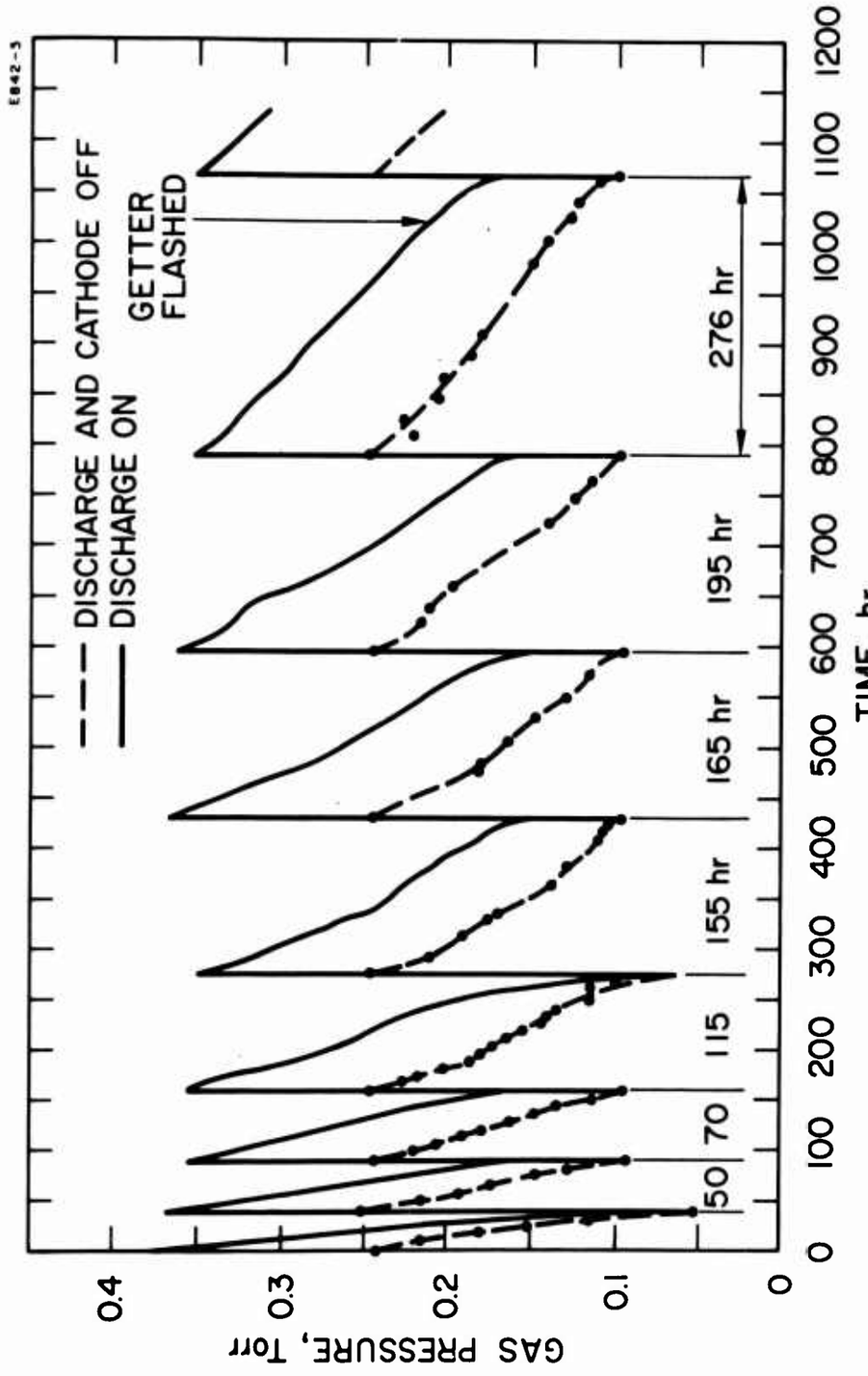

Fig. 6. Pressure variation with time for an oxide cathode at 20 A.

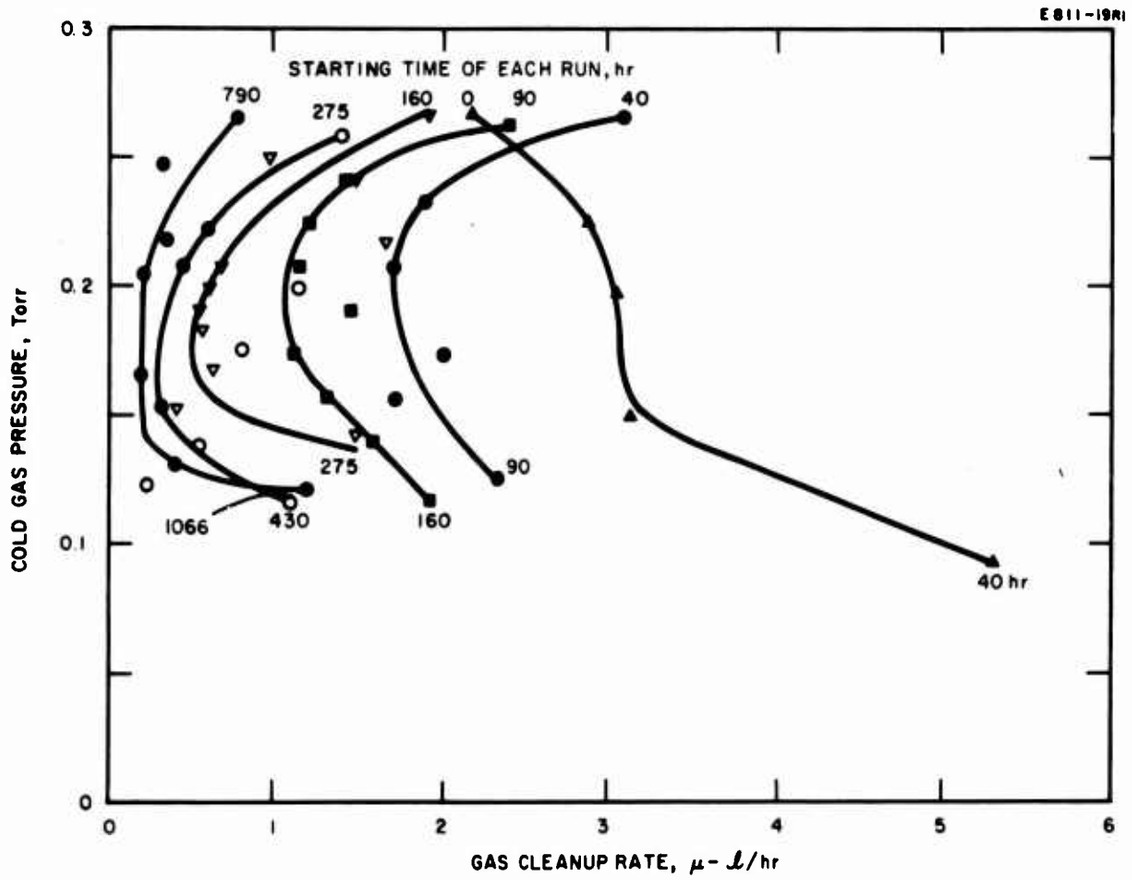

Fig. 7. Gas cleanup rate versus gas pressure during successive gas fills.

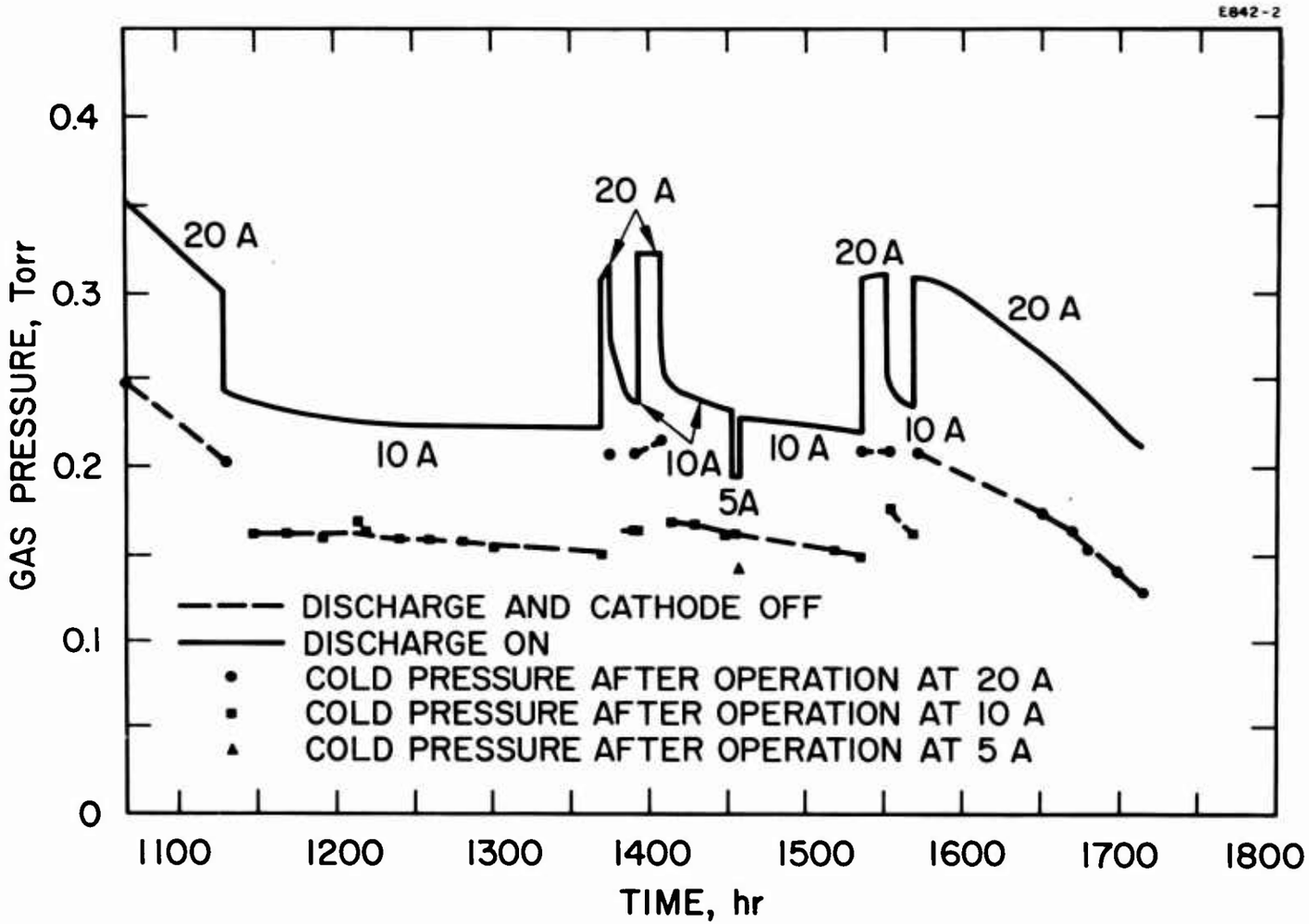

Fig. 8. Gas pressure versus time showing variation in pressure with discharge current.

decrease was not caused by contamination or leaks in the tube; the getter (which remained shiny and appeared unused throughout the run) was reflashed at 1025 hours, and no change in the gas pressure or GCR was observed.

The effect of gas pumping is evident from the difference in the hot and cold pressure readings at high and low filling pressures. The pressure gauge was mounted on the cathode bottle. In our gas pumping studies, we have determined that the anode to cathode pressure differential decreases as the gas pressure is reduced at constant I. This accounts for the observation in our cathode test that the hot tube pressure is ~0.11 Torr greater than the cold pressure at high pressures, and only ~0.06 Torr greater at low pressures.

We have based our calculation of GCR on changes in the cold pressure to avoid errors caused by gas pumping. The variation in GCR with pressure during each run is shown in Fig. 7. These curves were calculated from the daily change in cold gas pressure. For the sake of clarity, data have not been shown for the two runs between 430 and 790 hours; the GCR during these two runs fell between that of the preceding and following runs.

The gas cleanup behavior during the last 600 hours of the test is shown in Fig. 8. After the arbitrary requirement of 1000 hours at 20 A was satisfied, the discharge current was varied to observe the effect on the GCR.

The discharge was run at 10 A for 240 hours (1125 to 1365 hours). During this time the gas pressure decreased only 12 μ, yielding a GCR of 0.033 μℓ/hour, less than one tenth of the rate at 20 A. The strong dependence of GCR on I makes it clear that it is meaningful to compare the cleanup rates of different materials only if the discharge current is specified.

Another important observation is that large amounts of gas are absorbed in the walls and then re-emitted as the discharge current is varied. Note in Fig. 8 that the cold pressure after the tube has been operated at 10 A is 45 to 60 μ lower than after operation at 20 A. When the tube is again operated at 20 A, the gas is re-emitted and the cold gas pressure increases to the value previously recorded after operation at 20 A.

Measurements show that approximately 5 hours of operation at 10 A is required for the walls to absorb the gas and become saturated. The gas is all re-emitted in about 25 min when the current is increased to 20 A.

Approximately 20% of the gas in the tube can appear or disappear into the walls under different operating conditions. It is important to understand this behavior, especially if we wish to install an automatic gas replenishment system in future lasers to maintain the optimum gas pressure for lasing. Further experiments are planned.

F. Voltage-Current Characteristics

At the start of the experiment, the discharge voltage was 25 V and the filament was operated at 26 A ac and 2.1 V ac. During the test the tube voltage increased to a maximum of 35 V; when the electrical contacts were cleaned of oxidation, the voltage decreased to 27 and remained in the range of 27 to 29 V. The filament current was maintained at 26 A throughout the experiment; this required a gradual increase in the cathode voltage from 2.1 to 2.5 V ac.

G. Appearance of Cathode at End of Test

After 1715 hours of operation the test was terminated and the cathode inspected. The cathode was still operating satisfactorily at 20 A at the end of the test.

Figure 9 is a photograph of the front of the cathode with part of the heat shield cut away to expose the oxide coated mesh. Several observations may be made:

- The oxide coating is completely removed from the inner points of the mesh which are closest to the discharge. The mesh is still intact.
- Only a thin oxide coating is left on the mesh at the outer points.
- Ion sputtering has feathered the edge of the nickel heat shield. The edge of the innermost heat shield showed more damage than the edge of the outermost shield.

A second oxide cathode will be evaluated during the next quarter to provide statistical data on this type of cathode.

Fig. 9. Photograph of oxide cathode after 1700 hours of operation. Heat shield has been partially cut away to expose the nickel mesh.

III. BORE MATERIAL EVALUATION

The objective of this task (A.3 in Fig. 1) is to evaluate promising ion laser bore materials. Properties of interest are resistance to sputtering, cleanliness, gas cleanup, and thermal characteristics. Materials which are found to be the best will undergo further study in 1000 hour life tests (Task A.4).

Experiments using quartz, alumina, and segmented-bore molybdenum, tungsten, and graphite discharge tubes were conducted during the previous contract. Our conclusions regarding graphite were that, although it was ideal from the standpoint of resistance to localized damage, cost, machinability, emissivity, and thermal properties, it was not suitable for use in high power lasers (e.g. > 50 W/cm linear bore dissipation) because of powdering of the graphite. Graphite dust which collected between the segments and at the anode end of the tube did not affect operation of the discharge. However, the dust created a window contamination problem.

During the past quarter pure pyrolytic graphite (PG) and graphite overcoated with PG have been evaluated in 225 hour life tests. These materials look very promising; a small amount of powdering still occurs for both materials, but the powdering is one to two orders of magnitude less than that of regular graphite. Detailed information on the gas cleanup rate, output power, and durability of these materials is reported in this section.

A. Description of the Test Apparatus

Water-cooled quartz-envelope discharge tubes are used to support and maintain the alignment of the bore segments. Cooling of the segments is by radiation to the water jacket. Individual segments are 1/2 in. long with a 0.500-in. o.d. and 3 mm i.d., and are separated from each other by 1/16 in. diameter sapphire balls. The segments are made non-reentrant so that sputtering or powdering of the segments can be observed through the quartz envelope.

The 3 mm uniform bore region is 46 cm long; the bore constriction at each end of the bore consists of three 3/8 inch-long segments. The over-all length at the tube from window to window is 90 cm. A 120 cm radius high reflectance mirror and a 5% flat output mirror are used.

In these experiments the laser remains connected to the vacuum station through a Granville-Phillips leak valve with a metal-to-metal seal. A getter bottle and Hastings thermocouple gauge are connected to the laser. Gas replenishment to maintain the cold gas pressure within the desired operating range (0.15 to 0.3 Torr) is carried out by opening

the leak valve and adding gas to the existing fill whenever the lower pressure limit is reached.

B. Evaluation of Pyrolytic Graphite

1. Description of the Material*

Pyrolytic graphite is formed by deposition of carbon atoms on a hot (2000°C) substrate from hot flowing methane gas. The material has a layered structure similar to mica, and is highly anisotropic in its thermal and mechanical properties as shown in Table I. The C axis of PG is normal to the planar structure, so that the material is uniform and closely bound in the A-B plane, and layered along the C axis. The density is 2.2 g/cm^3, the theoretical maximum for carbon, compared with a density of 1.8 to 1.9 g/cm^3 for ultra-pure forms of graphite. The thermal conductivity in the A-B plane is excellent, while along the C-axis the conductivity is comparable with that of firebrick. We evaluated pyrolytic graphite because the higher density and tighter bonding of its carbon atoms might prevent the material from powdering. After discussions with carbon experts from Super Temp Corporation, a local company which is one of three commercial manufacturers of PG in the country, a set of bore segments was fabricated from 1/2 in. thick sheet PG. The C-axis of the material was aligned along the segment axis. Some of the characteristics of this material are apparent in the photographs shown in Fig. 10. Note the difference in the structure of the material when viewed along the A-B plane (Fig. 10(b)) and normal to this plane (Figs. 10(c) and (d)).

2. Operating Characteristics

The operating characteristics of the laser during the 220 hour test at 20 A discharge current are summarized in Fig. 11. The gas pressure and output power are plotted as a function of time. These data were taken over a 10 week period from 17 November 1966 to 27 January 1967.

The change in the pressure versus time characteristic at 145 hours was caused by air introduced (by mistake) into the tube during gas replenishment. Even though the tube was immediately pumped out, the getter was used up. The laser was operated for another 55 hours before the problem was diagnosed. Normal operating characteristics were again obtained at 200 hours when the getter was reflashed and the tube refilled.

---

*The general properties of graphite and PG were discussed in the final report of the preceding contract. The properties of PG are reviewed here to present a self-contained discussion of experiments with the material.

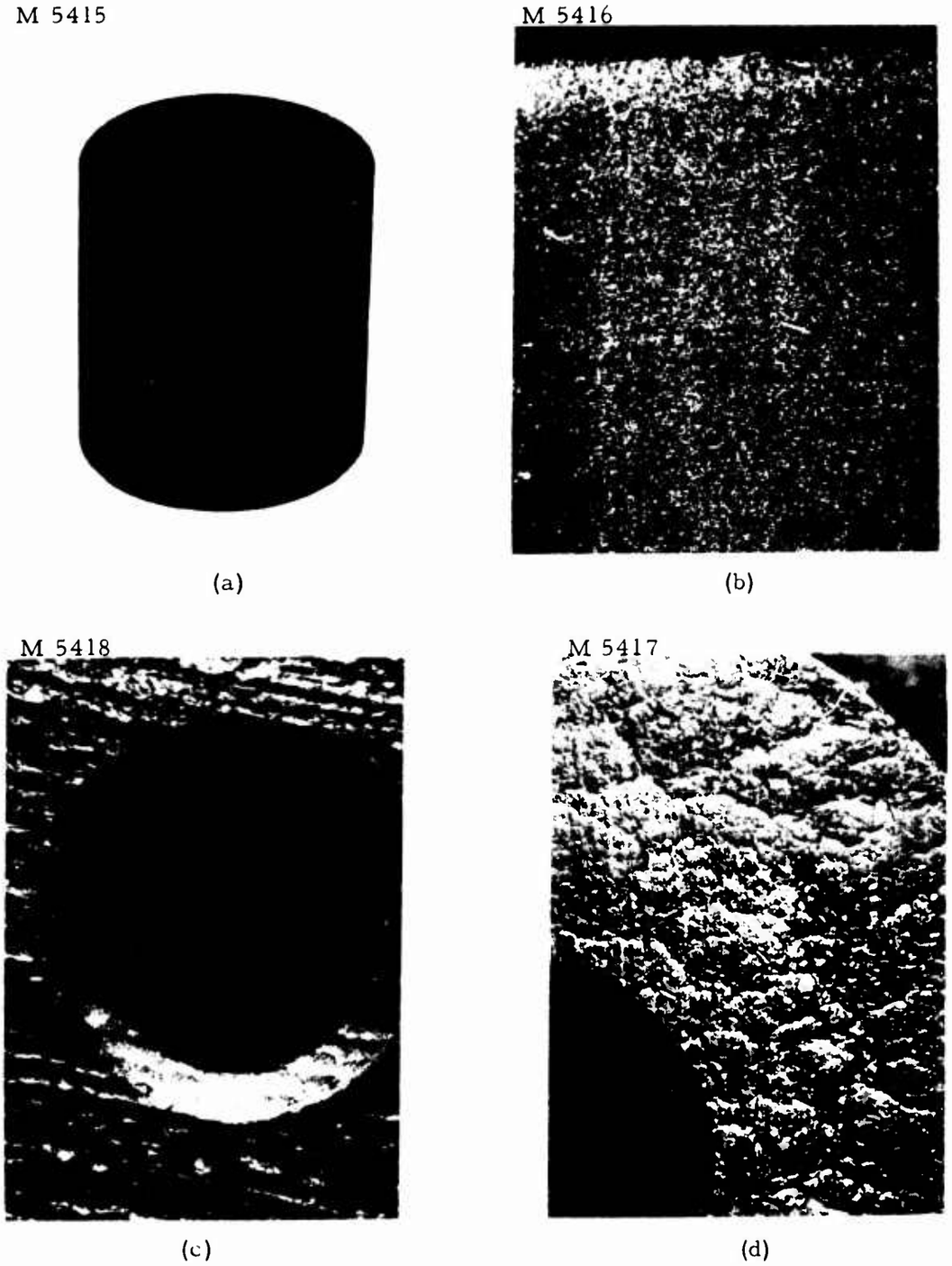

Fig. 10. Photographs of pyrolytic graphite segments. (a) Over-all segment appearance, (b) appearance of segment viewed along A-B planes, and (c) and (d) normal to A-B plane at 15x magnification.

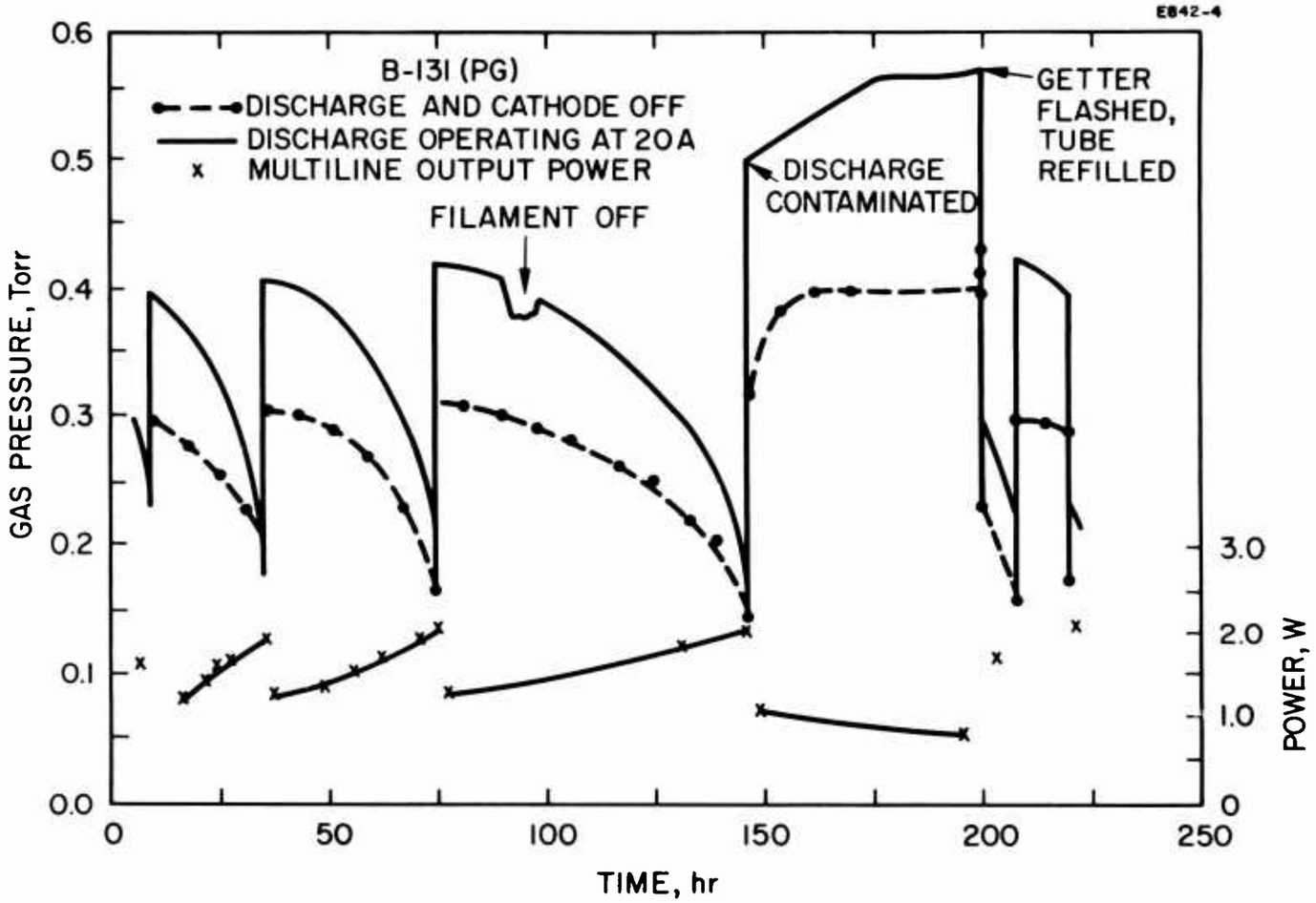

Fig. 11. Gas pressure and power output characteristics of tube B-131 versus time.

TABLE I

Comparison of Properties of Pyrolytic Graphite with Molybdenum and Normal Graphite at 1200°C

Property	Molybdenum	Normal Graphite	Pyrolytic Graphite	
			A-B	C
Density, g/cm^3	10.2	1.8-1.9	2.2	
Melting point, °C	2620	3500	3500	
Thermal Conductivity, BTU hour/ft^2/°F/in.	720	24	500	8
Thermal Expansion, 10^{-6} in./in./°F	3	2	0.25	12.5
Total Emissivity	0.37	0.8	0.85	0.5
Tensile Strength, lb/$in.^2$	2.5×10^4	4000	30,000	175

At 90 hours the filament supply power failed while the discharge was operating. The discharge tube continued to operate without heater power for 8 hours. No change in the tube voltage was noted. The filament supply was purposely turned on and off several times to verify this behavior. Evidently, once the tube is operating, heating of the oxide coating by the passage of the discharge current, or by ion sputtering, is sufficient to heat the coating to emission temperature.

Gas cleanup data, calculated from the change in cold gas pressure, is plotted in Fig. 12. Two trends are evident: (1) the GCR increases with decreasing pressure (with roughly a $1/p^3$ dependence), and (2) the GCR decreases with each gas fill (the cleanup rate during run 2 was roughly 2.5 times that of run 4).

The cleanup rate of the oxide cathode ranged between 1 and 3 $\mu\ell$/hour during the first 160 hours of operation (see Fig. 7), so the cleanup in the PG tube may occur at the cathode or anode rather than in the PG bore. More data on cleanup rates will be required before firm conclusions can be drawn.

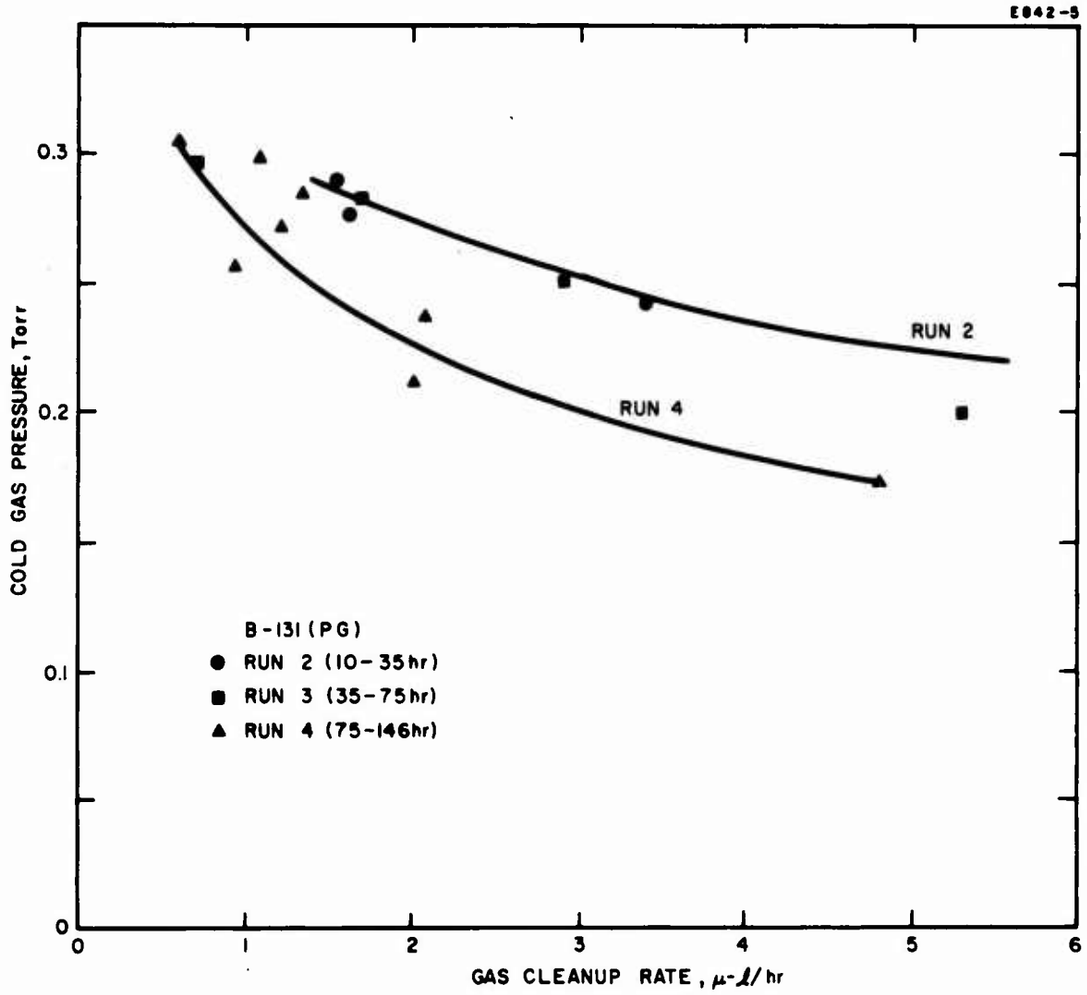

Fig. 12. Gas cleanup rate as a function of gas pressure during successive runs in tube B-131.

During the test the output power varied between 1.2 and 2.1 W with the low output occurring at high pressures, as expected. In all-quartz tubes we typically measure an output of 2 to 3 W at 20 A.

The lower curve of Fig. 13 shows the output power versus current as measured at the end of the experiment. At 35 A, 5.9 W was obtained. No window contamination problems were encountered.

The temperature of the radiation-cooled segments in the uniform bore was 1145°C at 20 A and 1365°C at 35 A. The hottest segment, in the cathode throat, was 1220°C at 20 A and 1436°C at 35 A. The low axial thermal conductivity of the PG was obvious from the temperature gradient in the throat segments which undergo nonuniform axial heating; the temperature of the anode end of one segment was > 100°C more than the cathode end of the same segment!

The tube voltage of the segmented PG tube ranged from 220 V at low pressures to 250 V at high pressures. This is approximately 40 V higher than the tube voltage of quartz bore tubes of the same length.

3. Resistance of the Material to Sputtering and Erosion

After 225 hours the tube was disassembled and the parts inspected for damage. Figure 14 is a photograph showing the appearance of the segments and the quartz envelope near the cathode end. The 1/16 in. diameter sapphire ball spacers are on the bottom of the tube. The first segment on the left is the first tapered segment in the cathode throat; experiments with molybdenum have shown that this segment is always the most severely damaged by sputtering. A buildup of graphite on the cathode end of the two segments on the right may be seen; the growth has fallen away from one of the segments. Figure 15 is a similar photograph of segments near the anode end of the tube.

Photographs illustrating features of the PG segments are shown in Fig. 16. Figure 16 (a) and (b) show the anode and cathode ends of typical bore segments. A buildup of graphite occurs on the cathode end of the segment. Figure 16 (c) shows exfoliation of the layers of the throat segment which reached the highest temperature. The layers were not separated on the far side of the segment where the sapphire ball pressed against the surface; we would not expect such layer separation to occur if there were a uniform pressure on the end of the segment.

The greatest deposit of carbon occurred at the anode end of the tube, as illustrated in Fig. 16 (d) and Fig. 15. From our earlier experiments with quartz-bore and molybdenum segment tubes, we know that wall damage does not occur in the bore near the anode, yet this is where the greatest accumulation of carbon is noted in all types of graphite bore tubes. Probable explanations for this are that either carbon particles become negatively charged and drift toward the anode, or gas flow carries the particles toward the anode.

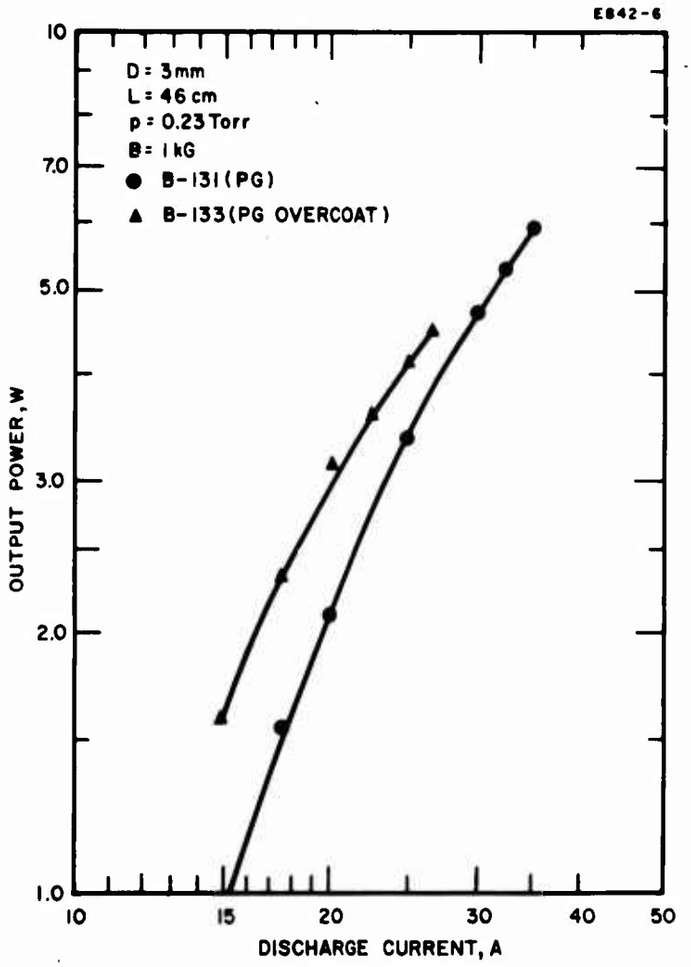

Fig. 13. Multiline output power versus discharge current for tubes B-131 and B-133 at end of test.

M 5331

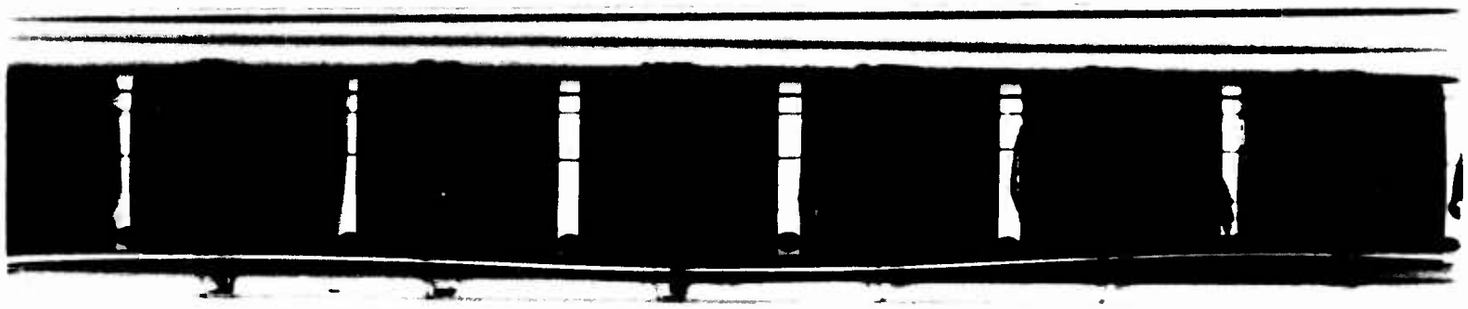

Fig. 14. Appearance of quartz envelope and bore segments at the cathode end of tube B-131 after 225 hours.

M 5332

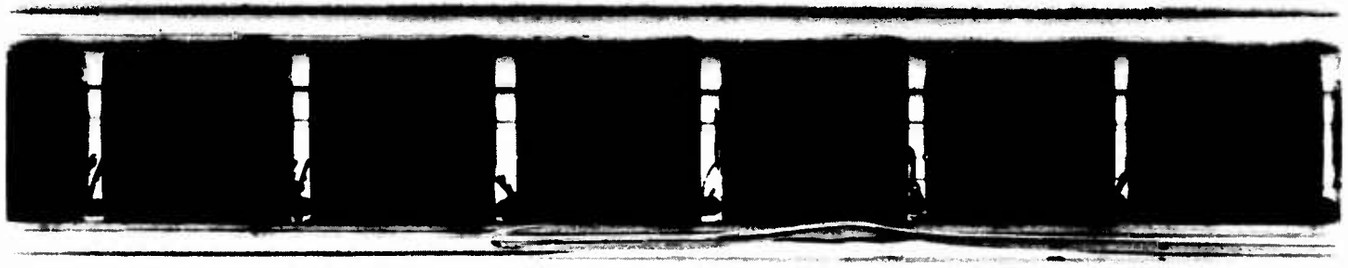

Fig. 15. Appearance of quartz envelope and bore segments at the anode end of tube B-131 after 225 hours.

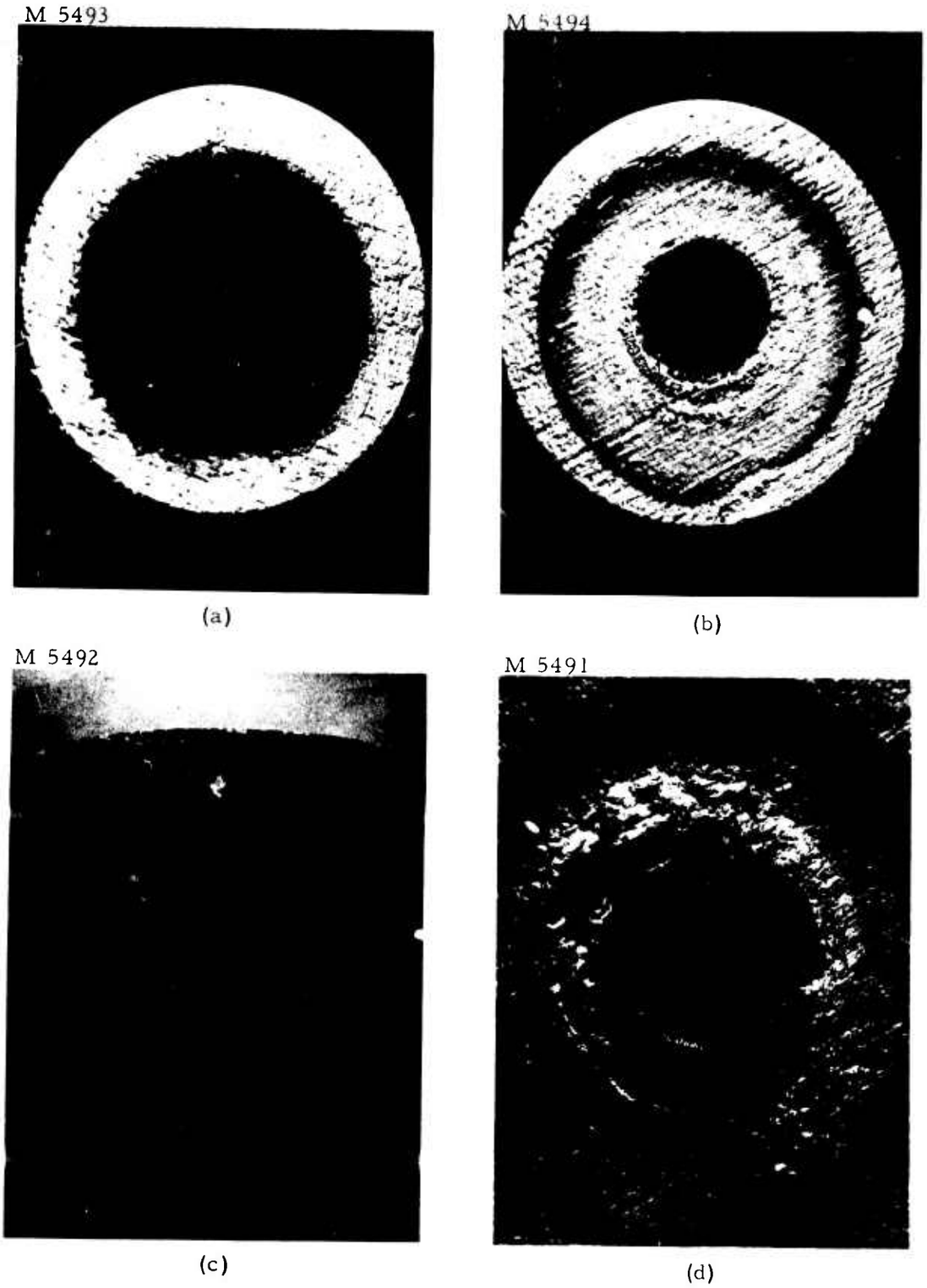

Fig. 16. Appearance of PG segments from B-131 after 225 hours (6x magnification). (a) Anode end, and (b) cathode end of typical bore segment. (c) Cathode throat taper segment showing exfoliation. (d) Cathode end of anode throat taper segment.

All the discoloration and carbon buildup on the segments, such as is shown in Figs. 16(a), (b), and (d), can be wiped off, leaving a clean surface such as is shown in Figs. 10(c) and (d). The edge of the bore is not eroded. The material in the carbon growths must therefore come from the inside bore surface. We could not detect a significant enlargement of the bore in any of the segments.

Our conclusions regarding pyrolytic graphite as a bore material are as follows:

- PG does not sputter or evaporate; there is no indication of material deposited on the walls.
- PG does not collect in the tube as dust in the same way that normal graphite does; rather, carbon particles build up as growths on the cathode end of each segment.
- Comparing the amount of graphite powder generated during 10 and 40 hour tests of normal graphite with that observed in the PG tube after 225 hours, we estimate PG powders at less than one tenth the rate of graphite.

C. Evaluation of Graphite with a PG Overcoat

1. Description of the Material

A second approach to improve the surface properties of graphite is to overcoat graphite with PG. This is done by heating the graphite segment to 2000°C and passing low pressure methane gas over the part. Pyrolytic graphite layers form, first infiltrating the existing surface, and then forming a thin PG overcoat. The PG structure is deposited with the C-axis normal to the surface, so that the layers follow the surface. The main advantage of this approach should be that the arc discharge bears upon a uniform surface in which each atom is tightly bound, rather than on the edge of the layers.

A set of bore segments was fabricated by overcoating spectroscopic grade graphite with a 0.005 ±0.001 in. PG coating. The appearance of the surface is shown in Fig. 17. The grooved texture of the o.d. resulted from a poor machine finish of the graphite. The i.d., which was reamed, was smooth.

The way in which the overcoat bonds to the segment may be seen in Fig. 18. Figure 18(a) shows an over-all view of the segment; the PG layer is just visible as a dark border. Figures 18(b) through (e) show the coating on different surfaces of the segments as viewed with polarized light at 400x magnification. The coating thickness is 0.0045 in. The

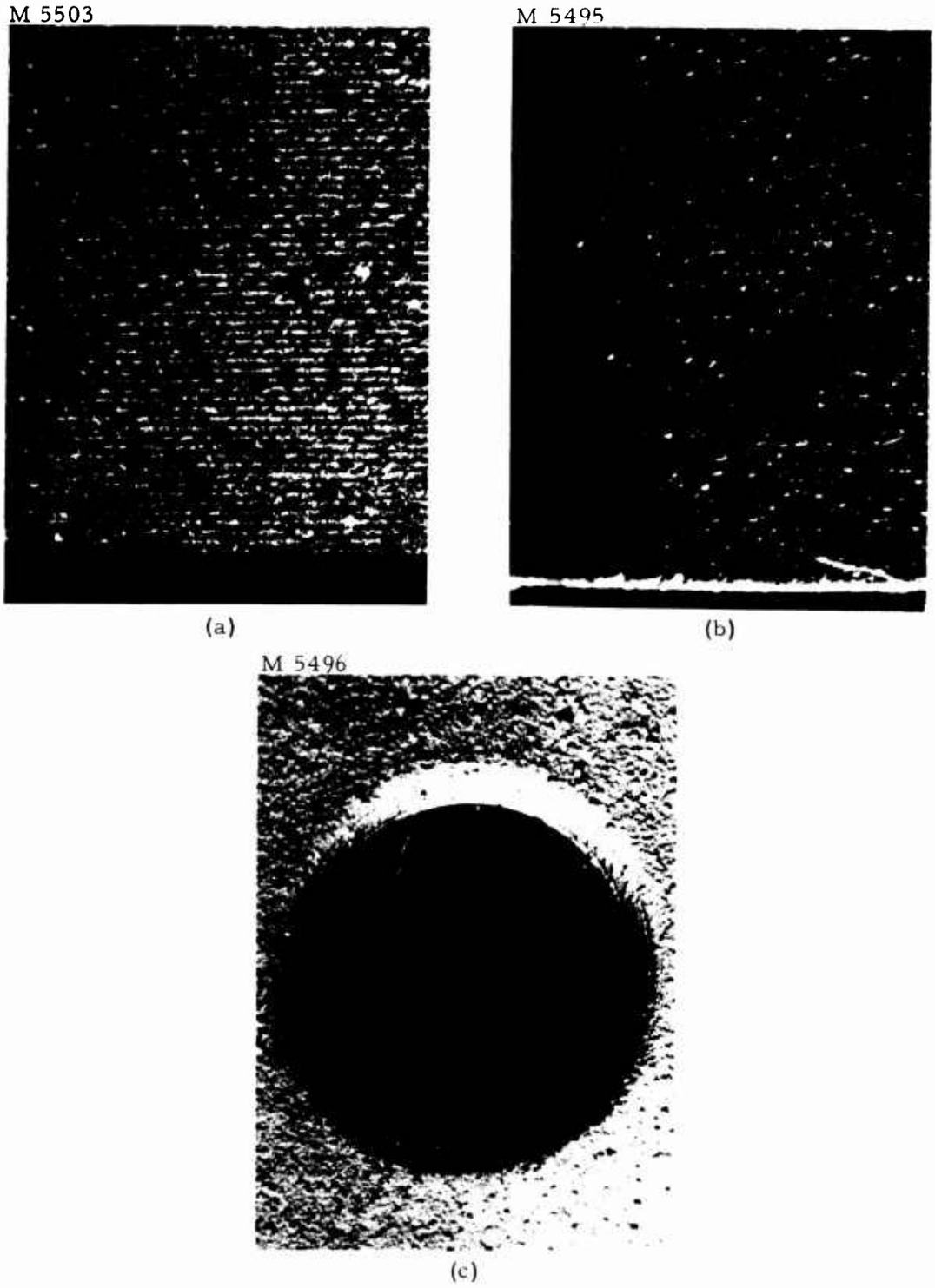

Fig. 17. Photographs of PG overcoated segments. (a) Side view of uncoated segment (15x magnification). Lines are machine marks. (b) Side view of overcoated segment. (c) End view of overcoated segment.

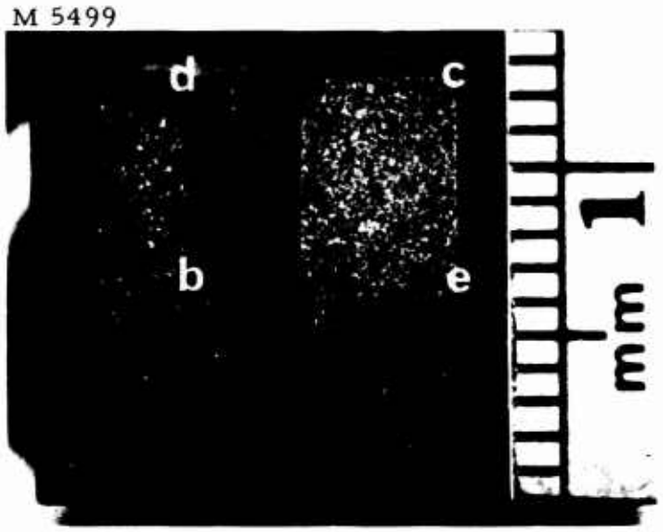

(a)

(b)

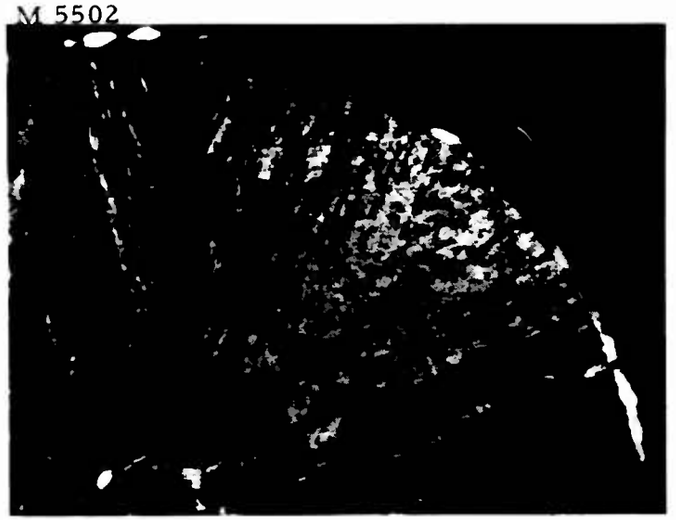

(c)

Fig. 18.
Cross section view of PG overcoated segments. (a) Cross section of segment at 5x magnification. Letters indicate regions shown in the higher magnification photographs which follow. (b) Cross section of coating in bore, 400x magnification. (c) Outside corner.

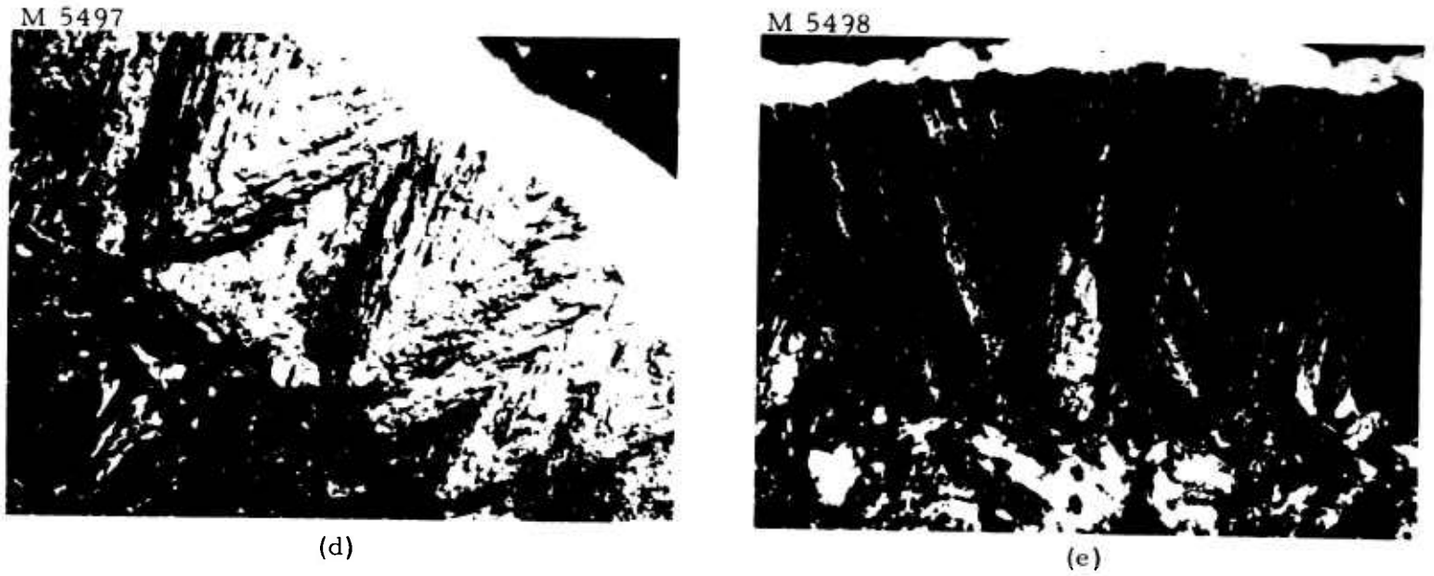

(d) (e)

Fig. 18 (cont'd). Cross section view of PG overcoated segments.
(d) Inside corner. (e) Outside surface.

homogeneity of the PG compared with the graphite is evident. Note the formation of growth cones in (d); the tops of these cones appear as bumps on the surface, as shown in Fig. 17(b) and (c).

2. Operating Characteristics

The operating characteristics of the tube are summarized in Fig. 19. The tube was operated at 20 A for 205 hours between 30 January and 28 March.

The GCR characteristics of the tube are plotted in Fig. 20. A comparison of the cleanup rate of tubes B-131 (Fig. 12) and B-133 show the rates to be very similar during the same period of operation.

The tube was operated for 7 hours at 10 A midway through the test. The same type of gas absorption and emission from the walls at different current levels was observed in the laser as in the cathode life test. Approximately 40 $\mu\ell$ of gas was absorbed into the walls during operation at 10 A. This gas was re-emitted when the tube was again operated at 20 A.

The output power cycled with pressure between 1.3 and 3.1 W at 20 A. At t = 38 hours the power was disappointingly low. The windows were sparked with a Tesla coil to see if performance could be improved. In the past, we have found that this sparking technique, which heats the window, has removed residue films which reduce output power or cause mode distortion. (Sparking does not remove particles from the window; in fact, it is likely to drive particles resting near the window up onto the windows.) A marked improvement in power was obtained, as indicated by the arrow at t = 38 hours in Fig. 19.

During the last 40 hours of the experiment the laser was being used as a source to study the beam divergence of low order transverse modes. After 205 hours the life test experiment was terminated and a new set of windows put on because a dust particle on the cathode window made it difficult to obtain TEM_{00} operation. The tube was run for an additional 25 hours at 20 A while additional beam divergence data were gathered. The power output characteristics of the tube at the end of test are shown in Fig. 13. The power output was 3.1 W at 20 A and 4.1 W at 25 A. This performance is as good as we have ever obtained from an all-quartz tube.

The tube voltage during the test cycled with pressure between 200 and 220 V.

3. Resistance of the Material to Sputtering and Erosion

The tube was disassembled and the parts inspected after 230 hours of operation at 20 A. Figures 21 and 22 show the appearance of the quartz envelope in the center of the tube and at the anode end. (The spring and tungsten wire arrangement shown in Fig. 22 allows

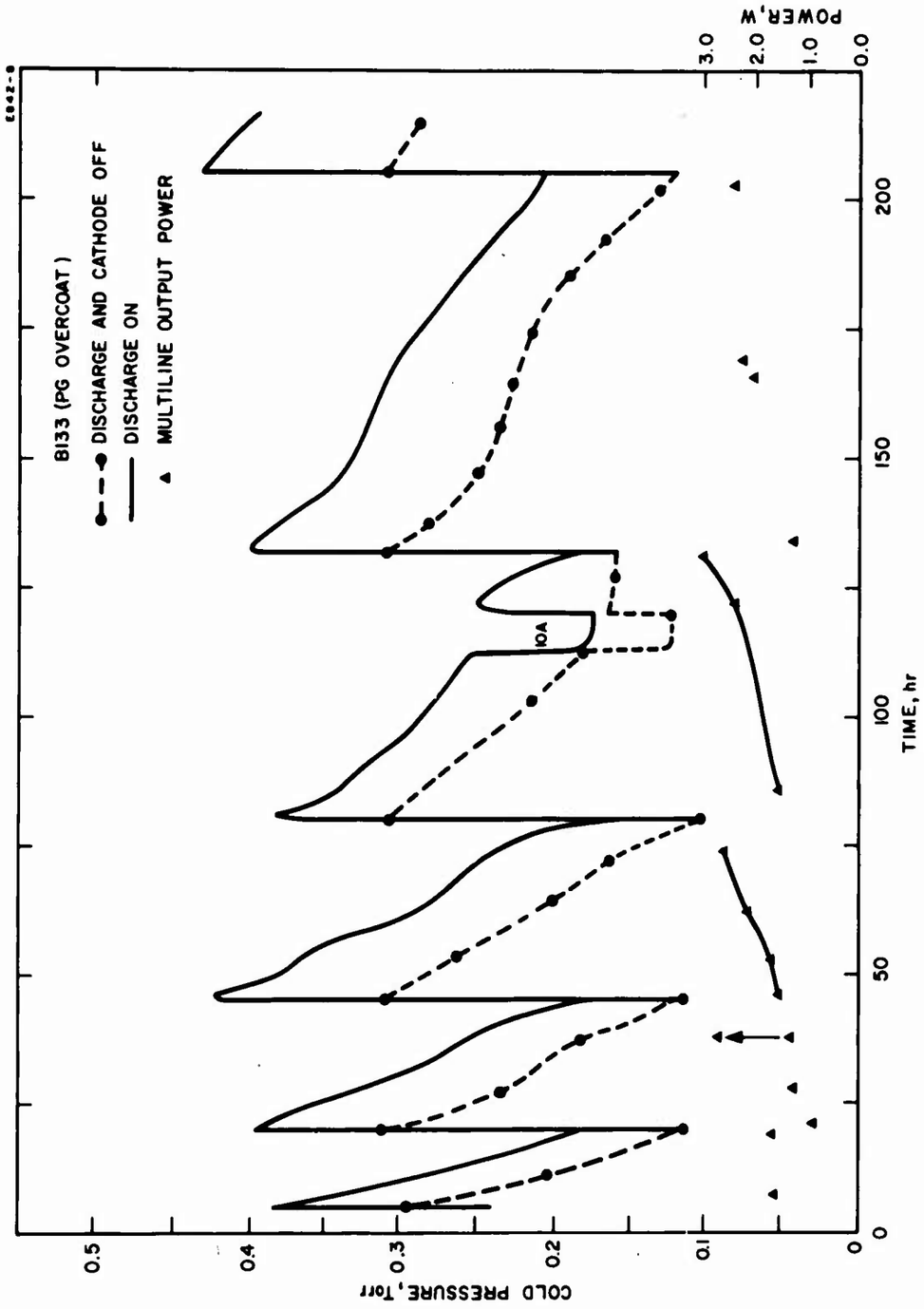

Fig. 19. Gas pressure and power output characteristics of tube B-133 versus time.

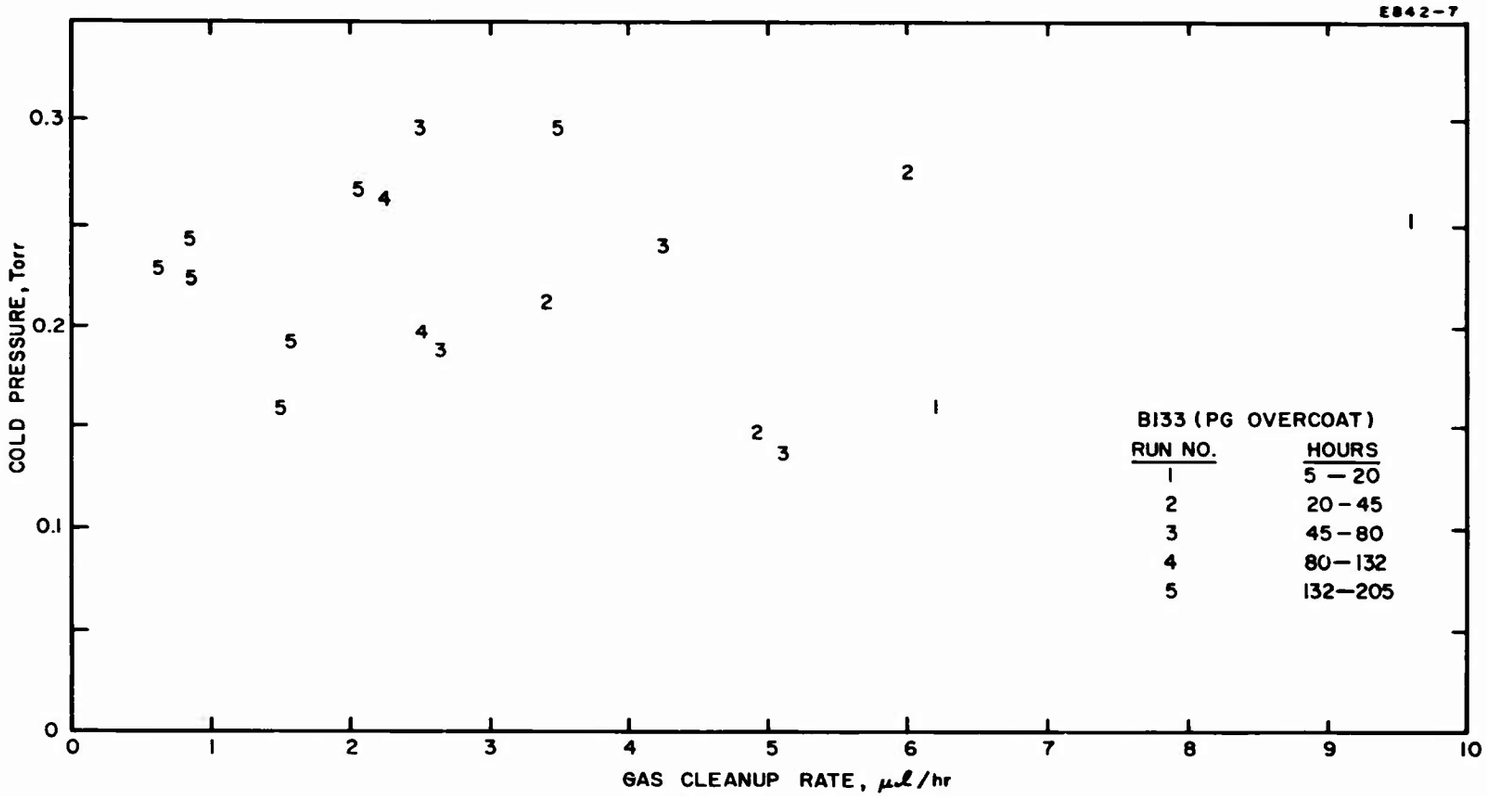

Fig. 20. Gas cleanup rate in tube B-133 as a function of gas pressure during successive runs.

M 5421

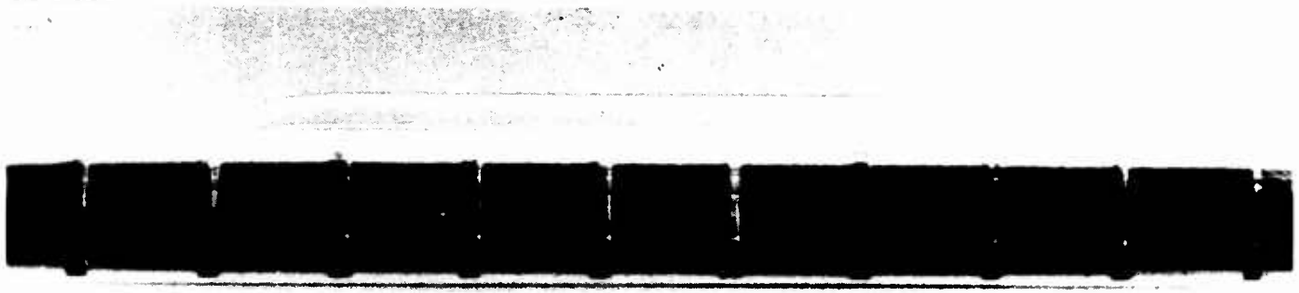

Fig. 21. Appearance of quartz envelope and bore segments at cathode end of tube B-133 after 230 hours.

M 5419

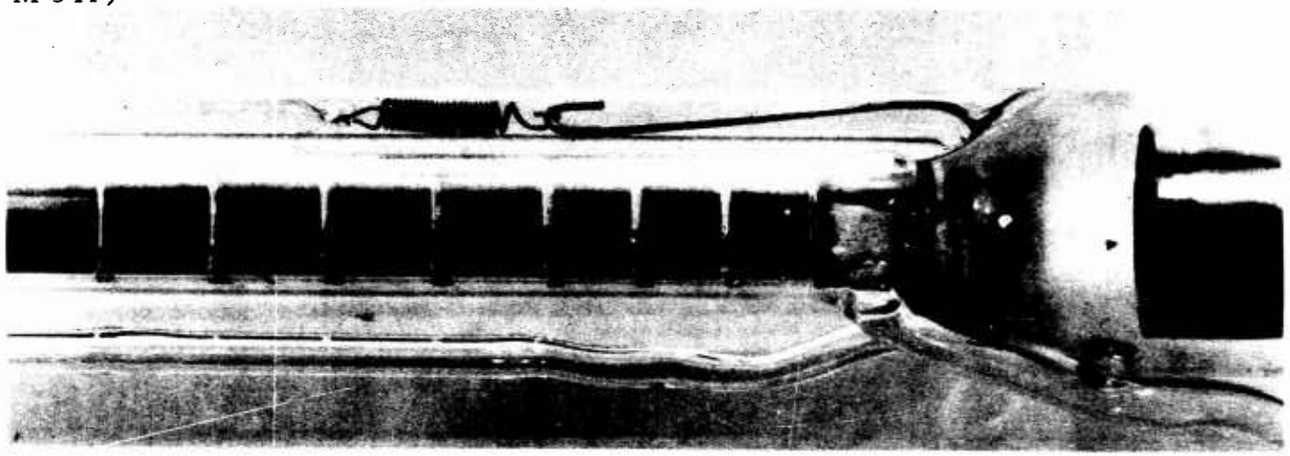

Fig. 22. Appearance of quartz envelope and bore segments at the anode end of tube B-133 after 230 hours.

longitudinal expansion of the segments toward the anode.) There was a slight discoloration of the envelope in the center of the tube, but otherwise this region was free of carbon dust. The concentration of carbon powder toward the anode end, commented on earlier, is clearly evident in Fig. 22.

Photographs of typical segments are shown in Fig. 23. There is some discoloration of the ends of the segments in the middle of the bore, as shown in (a) and (b), but no buildup of material. Figure 23(c) shows the segment at the anode end which had the largest accumulation of dust. All the carbon could be scraped from the segment, leaving the original surface.

Measurement of the i.d. of the segments revealed no erosion of the bore. The photographs of the PG overcoated segment shown in Fig. 18 are actually of a segment after it was run in the tube for 230 hours. The overcoating is of uniform thickness on all surfaces; erosion of as little as 0.0005 in. could have been detected easily if it has occurred. (The apparent axial change in the i.d. of the segment in Fig. 18(a) is caused by the sectioned plane being slightly tilted with respect to the axis, rather than by erosion.)

Our conclusions regarding the PG overcoated segments are similar to our comments on PG. Both materials are much better than regular graphite. Some difficulty with window contamination was noted with overcoated PG. The contaminating film could be removed by heating the window, and did not appear to be carbon dust.

Experiments to evaluate promising bore materials will be continued.

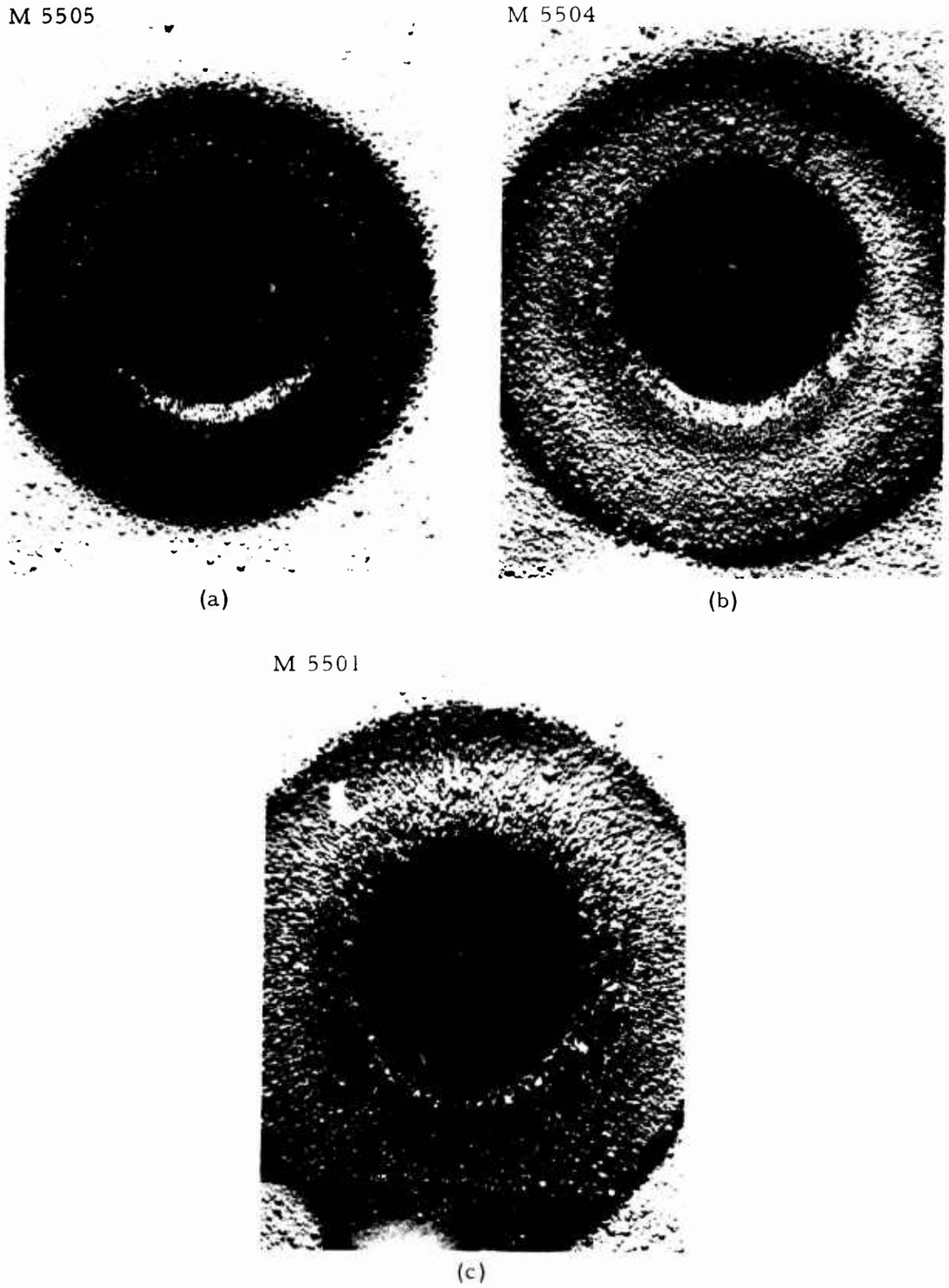

Fig. 23. Appearance of overcoated segments from tube B-133 after 230 hours (10x magnification). (a) Anode end and (b) cathode end of typical bore segment. (c) Cathode end of segment in the anode constriction.

IV. DEVELOPMENT OF A RADIATION-COOLED ANODE

The anode used in our cw ion lasers is a water-cooled, copper electrode mounted on hollow kovar pins which conduct both the coolant and the discharge current. The general design may be seen in the photograph of the cathode life test apparatus in Fig. 4. The anode is mounted on the axis of the tube to allow the tube to be inserted in a 2 in. i.d. solenoid. This design has proven simple and reliable. There are several disadvantages to this design, however:

- The coolant is in direct contact with the high voltage. Dielectric fluids or specially treated water must be employed to isolate the anode from ground. Electrolysis may cause material to be deposited in the copper coils, thereby reducing the coolant flow.

- The over-all diameter of the anode structure is 1-3/4 in. to accommodate the pins and window. This sets a lower limit on the i.d. of the solenoid. A reduction in the diameter of the anode would allow a smaller, lighter solenoid to be used.

- The over-all length of the anode from window to electrode is roughly 7 in. This length is required to accommodate the grade from 7052 glass to quartz.

- At very low gas pressures, the discharge extends through the anode. A high frequency, high voltage plasma instability develops simultaneously.

During the past quarter we have developed and tested a radiation-cooled anode for use in segmented bore tubes. The anode has been incorporated in a metal-ceramic segmented bore tube.

A sketch of the anode design is shown in Fig. 24. The last bore segment, which is inside the water jacket, serves as the anode. Electrical contact is made from the anode to the metal end piece through a flexible lead. The end piece is brazed to the ceramic envelope (in a metal-ceramic tube), or epoxied to quartz tubing.

A coil spring made of high temperature material is mounted between the anode and end piece. The spring allows axial expansion of the segments. The entire assembly from ceramic window support to anode segment is assembled as a unit and then inserted into the tube.

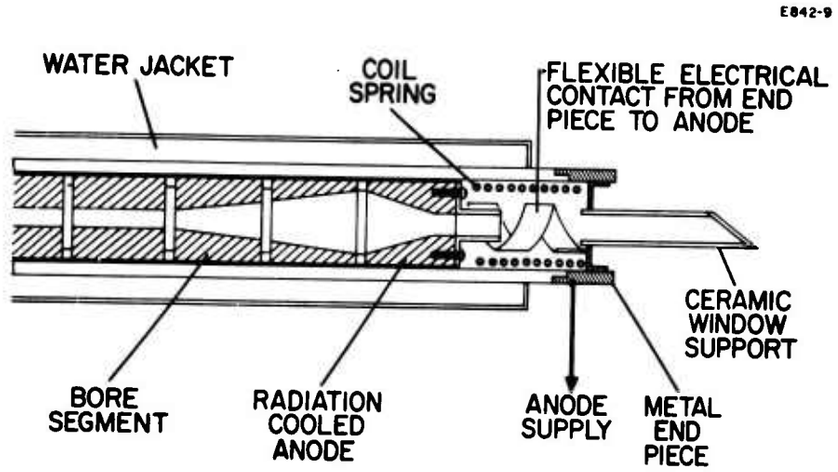

Fig. 24. Design of radiation cooled anode for segmented bore tubes.

This new design eliminates the problems of the water cooled anode. In particular, (1) high voltage is no longer in contact with the coolant, (2) the anode structure is the same o. d. as the bore so that a smaller, lighter solenoid may be used, (3) the over-all length from the anode to the window is only 3 to 4 in., and (4) provisions are made for axial expansion of the segments. The radiation-cooled anode was tested in a quartz envelope to see if any irregularities in the discharge near the anode occurred. The discharge was neatly collected in the anode cone and did not extend behind the anode.

V. NOISE STUDIES

More subtle demands on laser performance can be expected when reasonable lifetimes are obtained. One of these requirements is certainly to minimize noise modulation of the emitted beam. Fluctuations in the power output of an ion laser may be caused by:

1. ripple in the anode, solenoid, or filament supplies,
2. fluctuations in the active medium (the plasma) caused by instabilities in the discharge,
3. changes in the optical cavity loss or cavity length caused by movement of the mirrors or variation of the index of refraction of the air,
4. competition effects among different transverse modes or between adjacent cavity modes.

The goal of this study is to measure the noise contribution (amplitude and frequency spectrum) of each mechanism, and to minimize the noise modulation of the output. The effort this quarter has been to investigate beam noise introduced by power supply fluctuations. Measurements show that the total peak to peak (p-p) noise contribution from sources (2) through (4) above is <1% of the dc level; the modulation introduced by power supply ripple may easily exceed 10% unless special care is taken.

A. Power Supply Modulation of the Light Output

We wish to develop the transfer function which describes how power supply fluctuations couple to the light output. Power supply ripple will affect the laser output by modulating the excitation rate of the upper laser level population which, in turn, depends on the plasma density n_e and electron temperature T_e. The electron density and temperature interact with power supplies only through the discharge current I and the magnetic field B. Thus, we may write for the output power P

$$P(n_e, T_e) = P(I, B) \quad . \tag{2}$$

The modulation of P is therefore given by the relation

$$\frac{dP}{dt} = \frac{\partial P}{\partial B}\frac{dB}{dt} + \frac{\partial P}{\partial I}\frac{dI}{dt} \quad . \tag{3}$$

The first term on the right reflects the dependence of P on B at constant I; this dependence is illustrated in Fig. 25. Near the optimum magnetic field B_{opt}, the dependence of P on B may be approximated by the expression

$$P = P_{opt} - C_1(B - B_{opt})^2 \tag{4}$$

where C_1 is a constant which gives the best fit of (3) to the curves of Fig. 25 near B_{opt}. At 20 A for the curve shown, P_{opt} = 3 W, B_{opt} = 1.05 kG, and $C_1 \cong 2$ W/kG^2. For use in (3), we differentiate (4) to obtain

$$\frac{\partial P}{\partial B} = -2C_1(B - B_{opt}) \quad . \tag{5}$$

In the second term of (3), we know from parametric study data that

$$P = C_2 I^n \tag{6}$$

where n = 2 at high power levels (fully saturated medium), and $n \geq 4$ at low power levels. For a 3 mm bore tube at high powers, C_2 = 0.005 W/A^2.

The current ripple factor dI/dt in (3) must be expressed in a form which takes into account the power supply and circuit characteristics and that the discharge current can be modulated by the magnetic field. This latter dependence occurs because the tube voltage is a function of B. We therefore express dI/dt as

$$\frac{dI}{dt} = \frac{\partial I}{\partial B}\frac{dB}{dt} + \frac{\partial I}{\partial V_s}\frac{dV_s}{dt} \tag{7}$$

where V_s is the supply voltage. Figure 26 shows the equivalent circuit for the supply, ballant resistor R_B, and the tube which exhibits a current dependent resistance R_T. The internal resistance R_S of an ideal voltage supply is zero, while R_S for an ideal current regulated supply is infinite.

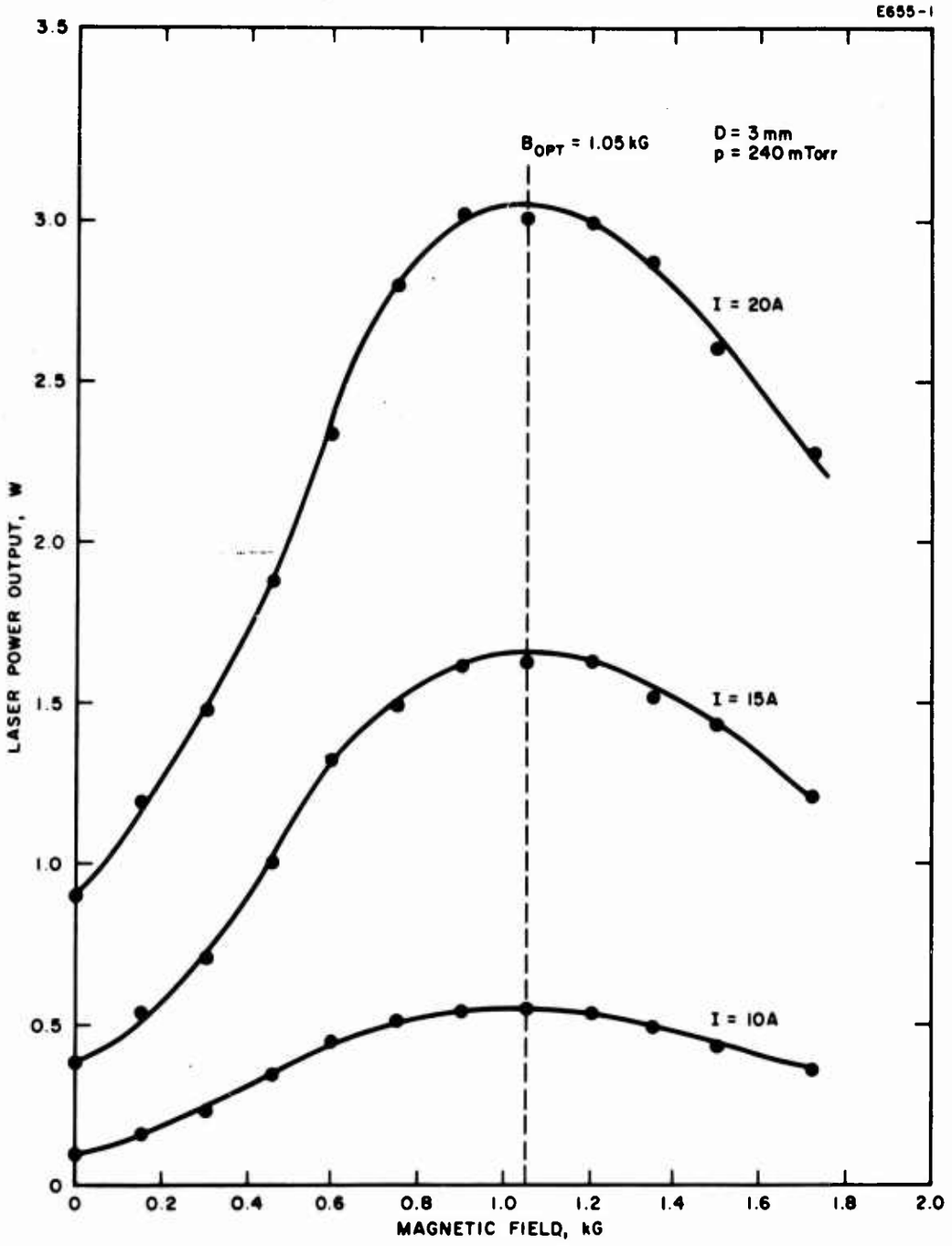

Fig. 25. Dependence of laser output power on magnetic field at constant discharge current.

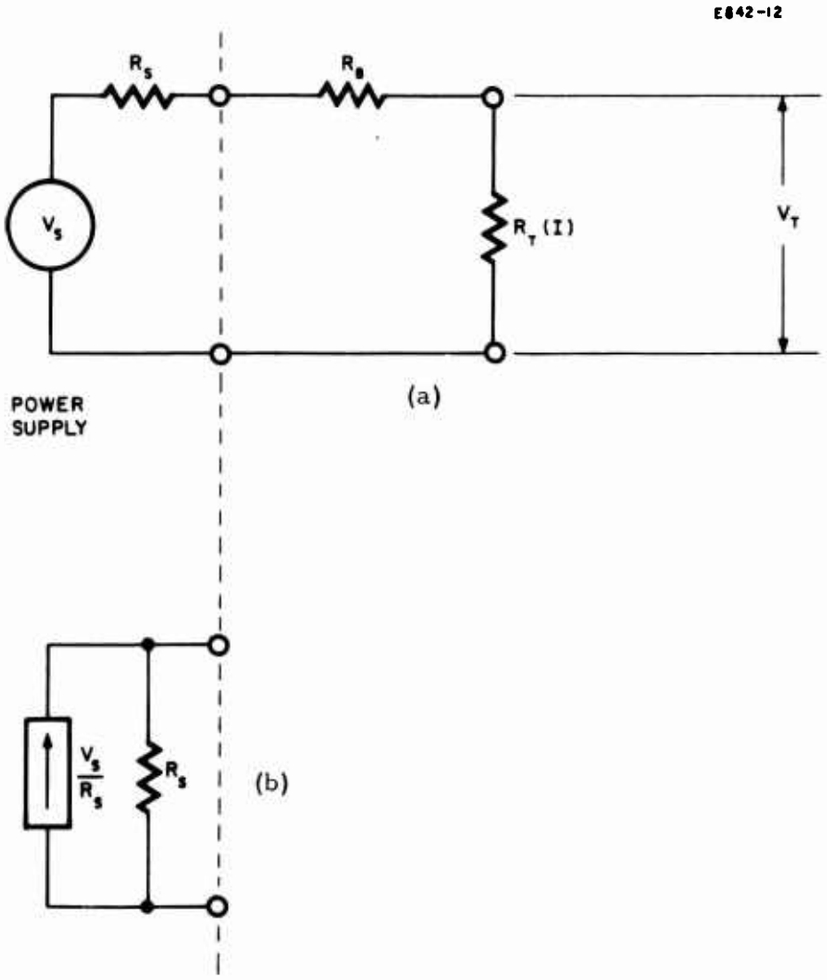

Fig. 26. (a) Equivalent circuit showing the relation of the power supply, ballast resistor, and discharge tube. (b) Equivalent circuit of a current regulated supply.

From Fig. 26,

$$I(R_S + R_B) = V_s - V_T \quad , \tag{8}$$

so that

$$\frac{\partial I}{\partial B} = - \frac{1}{R_S + R_B} \frac{\partial V_T}{\partial B} \quad . \tag{9}$$

The variation of V_T with B in a 3 mm tube at 15 A and 20 A is shown in Fig. 27. From these curves, $\partial V_T/\partial B$ = -30 V/kG at 0.8 kG and -11 V/kG at 1.0 kG. From (9), the larger $(R_S + R_B)$ is, the smaller will be the current modulation resulting from the dependence of V_T on B.

To express $\partial I/\partial V_S$ in (7) in the desired form, we differentiate (8) to obtain

$$\partial I(R_S + R_B) = \partial V_s - \frac{\partial V_T}{\partial I} \partial I \quad . \tag{10}$$

We recognize $\partial V_T/\partial I$ as the dynamic resistance of the tube,

$$\frac{\partial V_T}{\partial I} = R_{Tac} \quad . \tag{11}$$

Figure 28 illustrates the V_T versus I characteristics of a 4 mm tube. The slope of the curve at a given value of current is the dynamic resistance R_{Tac} at that particular value of current. For I > 20 A in a 4 mm tube of I > 12 A in a 3 mm tube, $R_{Tac} \cong 1\Omega$. Substituting (11) into (10) and rearranging terms yields

$$\frac{\partial I}{\partial V_s} = \frac{1}{R_S + R_B + R_{Tac}} \quad . \tag{12}$$

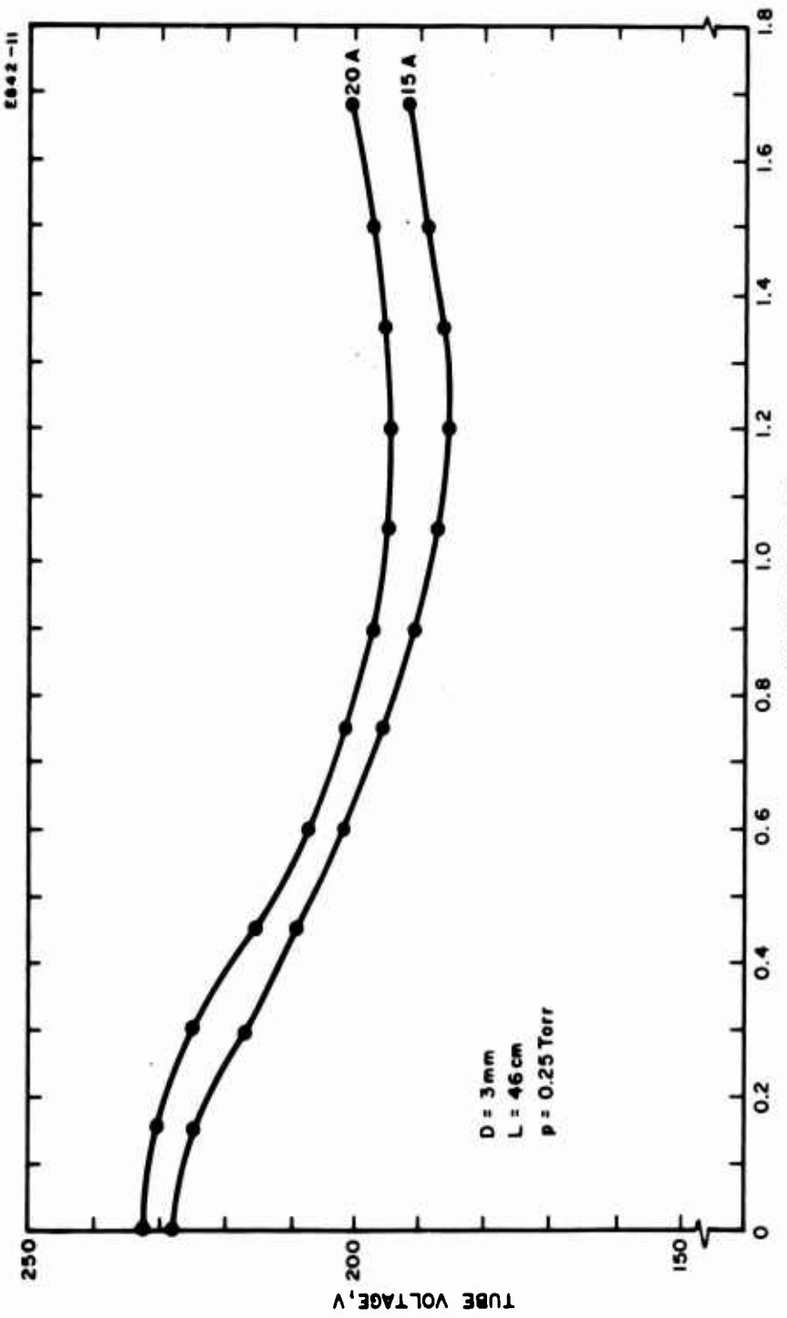

Fig. 27. Dependence of tube voltage V_T on magnetic field for two different values of discharge current.

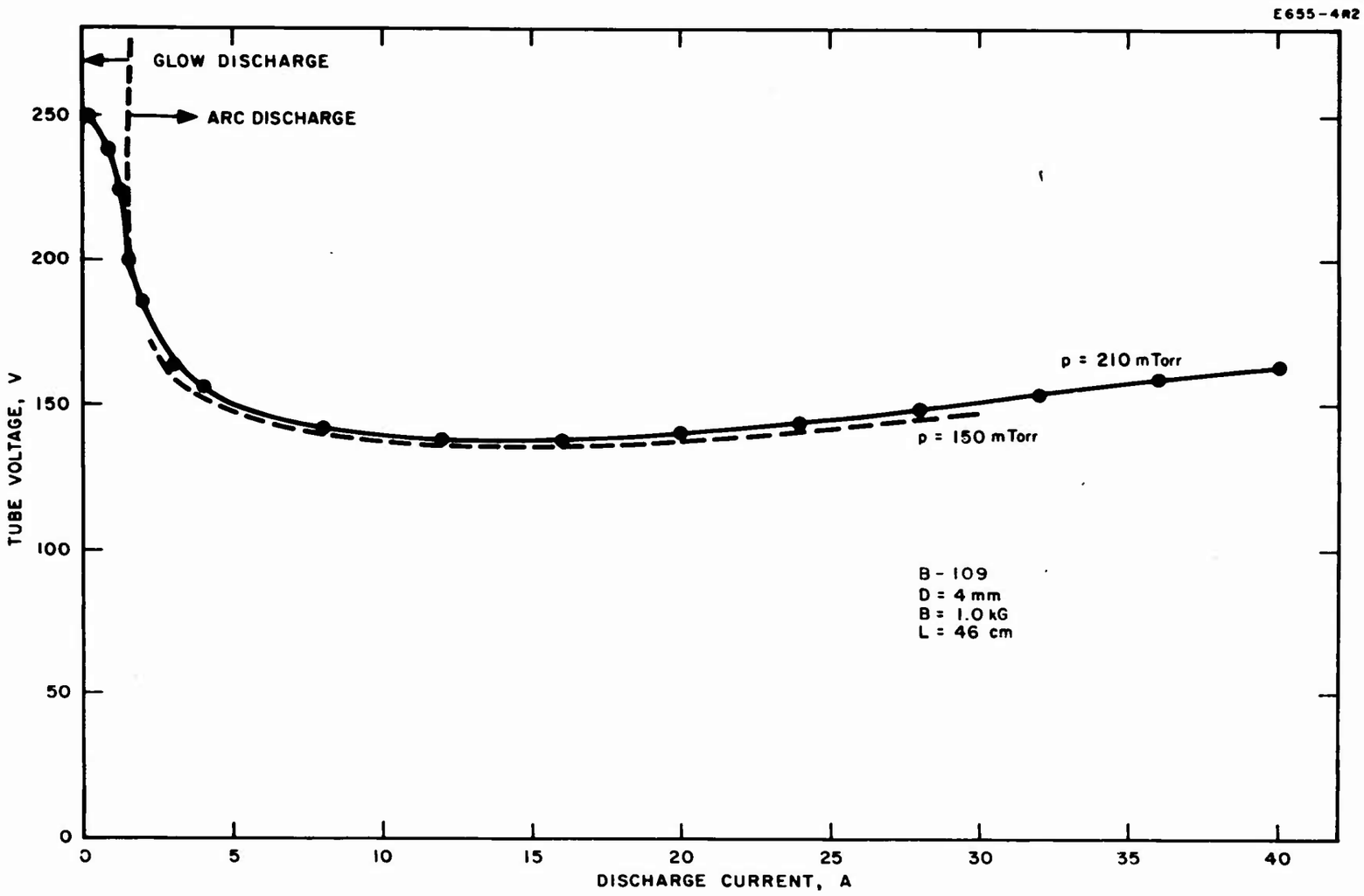

Fig. 28. Tube voltage versus discharge current at two different gas pressures for the 4 mm diameter tube.

Finally, introducing (7), (9), and (12) into (3) we obtain

$$\frac{dP}{dt} = \left[\frac{\partial P}{\partial B} - \frac{1}{R_S + R_B}\frac{\partial P}{\partial I}\frac{\partial V_T}{\partial B}\right]\frac{dB}{dt} + \left[\frac{1}{R_S + R_B + R_{Tac}}\frac{\partial P}{\partial I}\right]\frac{dV_s}{dt} \tag{13}$$

which is the desired transfer function coupling power supply ripple to modulation of the output. Numerical values for the coefficients $\partial P/\partial B$, $\partial P/\partial I$, $\partial V_T/\partial B$, and R_{Tac} may be obtained from tube operating characteristics as discussed above.

B. Selection of Power Supplies

1. Current Regulated Supplies

Since the output power is a function only of discharge current and magnetic field, it is clear that beam modulation will be minimized when low ripple, current regulated supplies are used to drive the discharge and solenoid. For this case, from (3), or from ~~(12)~~ (13) with $R_S = \infty$,

$$\frac{dP}{dt} = \frac{\partial P}{\partial B}\frac{dB}{dt} + \frac{\partial P}{\partial I}\frac{dI}{dt} \quad . \tag{3}$$

If an output power P_o is obtained with a dc current I_o and a dc magnetic field B_o, then, from (6),

$$C_2 = \frac{P_o}{I_o^n} \quad , \tag{13}$$

so

$$P = \frac{P_o}{I_o^n} I^n \quad , \tag{14}$$

and

$$\left.\frac{\partial P}{\partial I}\right|_{I_o} = \frac{nP_o}{I_o} \quad . \tag{15}$$

The fraction change in P_o caused by a ripple in B or I may be expressed by dividing (3) by P_o and introducing (15) to obtain

$$\frac{I}{P_o}\frac{dP}{dt} = \left(\frac{B_o}{P_o}\frac{\partial P}{\partial B}\right)\frac{1}{B_o}\frac{dB}{dt} + n\frac{1}{I_o}\frac{dI}{dt} \quad . \tag{16}$$

From the second term of (16) it is evident that the peak-to-peak (p-p) beam modulation of a laser operating in the $P \sim I^n$ regime due to the ripple of a constant current anode supply will be n times the p-p anode power supply ripple. For high power lasers, n = 2.

A quick calculation of the quality $(B_o/P_o)\,\partial P/\partial B$ in (16) from the data of Fig. 25 shows that this coefficient is $\ll 1$ for B_o near B_{opt} and reaches a maximum of 0.7 at $B_o/B_{opt} = 0.6$. The ripple requirements on a current regulated solenoid supply are therefore much less stringent than on the anode supply.

Suitable current regulated SCR power supplies are now becoming available* which claim to have a maximum RMS ripple of 0.15% . It should therefore be possible to maintain the RMS ripple of the light beam at <0.4% . It is not possible to estimate the corresponding p-p ripple without knowledge of the current waveform.

2. Voltage Regulated Supplies

Our laboratory ion laser power supplies are voltage regulated units using diode rectifiers. Solenoid supplies employ a standard 3ϕ bridge circuit which should have a 4.2% RMS and a 14% p-p ripple; we measure a 13% p-p ripple. Anode supplies utilize a 3ϕ transformer with a dual Δ - Y secondary so that 6ϕ rectification may be used. Capacitive filtering of the output reduces the ripple to 2% p-p. The high current, low impedance characteristics of the discharge make it difficult to reduce the ripple further.

*For example, H-P Model 6479A, or Rowan Model SCR 250-40.

We shall now consider the output modulation when such voltage supplies, which have p-p ripples of > 2%, are used. (SCR supplies with lower ripple may be employed, of course, but such supplies generally can be operated as constant current sources.)

Introducing (15) into (12) and using the relation

$$V_s = I(R_S + R_B + R_T) \quad , \tag{17}$$

the fractional change in power output caused by changes in B and V_s may be expressed as

$$\frac{I}{P_o}\frac{dP}{dt} = \left[\frac{B_o}{P_o}\frac{\partial P}{\partial B} - \frac{n\,B_o}{(R_S + R_B)\,I}\frac{\partial V_T}{\partial B}\right]\frac{1}{B_o}\frac{\partial B}{\partial t}$$

$$+ \left[\frac{n(R_S + R_B + R_T)}{R_S + R_B + R_{Tac}}\right]\frac{1}{V_s}\frac{dV_s}{dt} \tag{18}$$

Considering first the effect of fluctuations in V_s, we note that for a ~~current~~ voltage regulated supply the modulation of the output is n times the ratio of the dc to ac resistance times the power supply ripple. Typical values of resistance are $R_S = 0.5\ \Omega$, $R_T = 10\ \Omega$ (in a 3 mm tube at 20 A), and $R_{Tac} = 1\ \Omega$, so that

$$\frac{R_S + R_B + R_T}{R_S + R_B + R_{Tac}} \cong \frac{10.5 + R_B}{1.5 + R_B} \quad . \tag{19}$$

Obviously, a large ballast resistor is required if ripple is to be minimized; this is, of course, equivalent to adding a large series resistance to approximate a constant current supply. If we require that the ballast resistor dissipate no more power than is dissipated in the discharge, then $R_B = R_T \cong 10\ \Omega$. For this case, from (18)and(19), the output modulation will be $n(20.5/11.5) = 1.8\ n$ times the power supply ripple. This multiplication factor will be 3.6 at high powers.

The two terms which comprise the coefficient of the magnetic field ripple term may be evaluated from the data shown in Figs. 25 and 27. The magnitudes of the two coefficients are compared in Table II for the case of a 3 mm tube at 20 A; power was taken to vary as I^2. The relative sizes of the two terms will depend on the value of $(R_S + R_B)$; typically, the sum of these resistances is in the range of 3Ω to 10Ω. As an example, if $B_o/B_{opt} = 0.8$, and $(R_S + R_B) = 10\ \Omega$, the magnetic field ripple coefficient would be $(0.4 + 1.9/10) = 0.6$, and the output beam would have 0.6 of the ripple of the solenoid supply.

For $B_o \approx B_{opt}$, we conclude that the ripple transferred from the magnetic field to the output beam is much less than that caused by fluctuations in V_s.

TABLE II

Magnetic Field Ripple Coefficients in Eq. (18)
for a 3 mm Tube at 20 A

B_o/B_{opt}	B_o (kG)	$\left[\frac{B_o}{P_o}\frac{\partial P}{\partial B}\right]$	$-\left[\frac{n\,B_o}{(R_S + R_B)I}\frac{\partial V_T}{\partial B}\right]$ with n = 2, I = 20 A
0.4	0.42	0.6	$2.6 \div (R_S + R_B)$
0.6	0.63	0.7	$2.6 \div$ "
0.8	0.84	0.4	$1.9 \div$ "
1.0	1.05	0	$0.3 \div$ "
1.2	1.26	-0.2	$-0.6 \div$ "
1.4	1.47	-1.0	$-1.8 \div$ "

C. EXPERIMENTAL RESULTS

The best method to verify the power supply ripple-output modulation relationships developed above would be to employ low-ripple supplies, introduce a known amount of ripple in B, I, or V_s, and measure the resulting beam modulation. Unfortunately, low-ripple solenoid and

discharge current supplies were not available in our laboratory during the past quarter. However, suitable constant current supplies were available in an argon laser system built here over a year ago and now installed at a HAC Culver City facility. Noise measurements made thus far have been on this system. The major difficulty in carrying out the measurements is that the filament, solenoid, and anode supplies are integrated into a common 400 Hz supply with intricate cabling to the laser head. This makes it rather difficult to monitor supply characteristics. The results reported below are in agreement with predicted behavior, however.

The characteristics of the solid state, 400 Hz supply are as follows:

Filament Supply: 2.2 V dc at 25 A with a p-p modulation of 7%. The modulation consists of 10 μsec pulses at a 100 μsec prf.

Solenoid Supply: 120 V dc at 10 A ($B_o = B_{opt} = 1$ kG) with a 1.25% p-p ripple at 200 Hz.

Anode Supply: Current regulated, 20 A, with a 0.5% current ripple at 200 Hz when driving the discharge.

When the laser was operated at 18 A discharge current, the modulation of the output was 1% p-p at 200 Hz. This is in agreement with the behavior predicted in Section V-B-1 when the magnetic field is near the optimum and the tube is operated at high powers.

The random noise modulation of the beam – that is, the modulation not clearly identified by frequency as fluctuations caused by power supply ripple – was 0.4%.

A 60 Hz, single phase solenoid supply with a 20% p-p ripple at 120 Hz was substituted for the low-ripple solenoid supply to observe the degree to which magnetic field ripple was transferred to the output beam. A 1% p-p modulation of the beam at 120 Hz was measured; this is a transfer of 0.05 of the B field ripple to the beam.

A 60 Hz ac filament power was applied to the hot oxide cathode. Low-ripple supplies were used for the solenoid and anode. The output beam had a 60 Hz, 29% p-p modulation at a discharge current of 15 A, and a 12% modulation at 18A. This ripple is caused by the ac variation in the potential of the directly heated cathode mesh with respect to the anode, and not by a periodic change in the emission characteristics of the cathode. (The cathode temperature could not change that rapidly, and in addition such a change would occur at a 120 Hz rate, rather than an observed 60 Hz.)

The variation in cathode potential is equivalent to varying V_s. We would not expect this variation to modulate the output when a constant current supply is used. It may be that the response time of the anode supply is greater than 16 msec, in which case the supply would behave like a constant voltage source to a 60 Hz variation.

One side of the cathode mesh is common to the negative lead of the anode supply. The other side will vary over a range of $\pm 2.2\sqrt{2} = \pm 3.1$ V with respect to the negative side. If we consider the average p-p variation in cathode potential to be 3 V, which is the change in potential of a point midway between the cathode terminals, then the ac circuit resistance which would allow a 29% to 12% modulation of the beam may be calculated. A 29% modulation of the beam at 15 A indicates a 14.5% modulation of the current, or a p-p ripple of 2.2 A. The ac circuit resistance at 15 A is therefore $3V/2.2A = 1.4\Omega$. The ac resistance at 18 A would be 1.5Ω.

D. CONCLUSIONS

Analysis and measurements of fluctuation in the output beam indicate the dominant source of beam modulation will be power supply ripple. Other sources of noise amounted to only a 0.4% beam modulation for the particular laser considered.* Additional measurements will be carried out to verify the transfer function of power supply ripple to beam modulation.

*This conclusion also applies to induction excited lasers; specifications on the Spectra-Physics Model 140 argon ion laser quote a beam ripple of < 10% at 360 Hz, < 2% at 20 to 23 MHz (the excitation frequency), and beam noise of < 1% in the range of 10 to 100 kHz

VI. PLANS FOR THE NEXT QUARTER

The areas of study during the next quarter are indicated in Fig. 1. Cathode and bore material evaluation will continue. The design of segmented-bore tubes will be studied with particular emphasis on the dependence of power output, efficiency, and erosion on the length and spacing of segments. The merits of using permanent magnets to replace the solenoid will be investigated.

VII. PERSONNEL QUALIFICATIONS

The qualifications of Dr. Robert J. Freiberg who recently joined our staff are outlined below. Dr. Freiberg will devote part of his time to this contract in the future.

ROBERT J. FREIBERG, Member of the Technical Staff, Electron Device Physics Department, Hughes Research Laboratories.

Education — B. S. (Physics), Renssalaer Polytechnic Institute, 1961; M. S. (Physics), University of Illinois, 1963; Ph. D. (Physics), University of Illinois, 1966.

Experience — Dr. Freiberg joined Hughes Research Laboratories in January 1967. He is presently engaged in research on ultraviolet ion lasers and cavity and beam characteristics of argon ion lasers.

While at the University of Illinois, Champaign, Illinois, he conducted research on noble gas lasers operating at visible and infrared wavelengths, with particular emphasis on the physical mechanisms associated with electron-excited atom interactions.

During the summers of 1961 and 1962, Dr. Freiberg was employed by the Physics Department of the Argonne National Laboratories, Argonne, Illinois, as a Research Associate where he investigated basic processes occurring in high frequency, low pressure plasmas and plasmoids.

Honors — Sigma Xi, Renssalaer Polytechnic Institute Scholarship (1957 through 1961), National Science Foundation Graduate Cooperative Fellowship (1965 and 1966).

Professional Societies — American Physical Society, IEEE.

Publications — Dr. Freiberg has published several papers dealing with gas lasers and gaseous plasmas.

REFERENCES

1. G. A. Haas, "Thermionic Electron Sources," NRL Report 5657, U. S. Naval Research Laboratories, Washington, D. C., 6 Oct 1961.

2. K. G. Hernquist and J. R. Fendley, Jr. "Construction of long life argon lasers," J. Quantum Electron. QE-3, 66 (1967).

3. I. Gorog and F. W. Spong, "Experimental investigation of multi-wall argon lasers," RCA Rev. 28, 38 (1967).

4. G. A. Haas and J. T. Jensen, Jr., "Use of oxide cathodes in demountable vacuum systems," Rev. Sci. Instr. 28, 1007 (1957).

Unclassified

Security Classification

DOCUMENT CONTROL DATA - R&D

(Security classification of title, body of abstract and indexing annotation must be entered when the overall report is classified)

1 ORIGINATING ACTIVITY (Corporate author) Hughes Research Laboratories 3011 Malibu Canyon Road Malibu, California 90265	2a REPORT SECURITY CLASSIFICATION Unclassified 2b GROUP N/A

3 REPORT TITLE

Gaseous Ion Laser Research

4 DESCRIPTIVE NOTES (Type of report and inclusive dates)

Interim Technical Report – 1 January 1967 through 31 March 1967

5 AUTHOR(S) (Last name, first name, initial)

Halsted, A.S., Bridges, W.B., Friedrich, H.R.

6 REPORT DATE	7a TOTAL NO. OF PAGES	7b NO. OF REFS
May 1967	61	7

8a CONTRACT OR GRANT NO. b. PROJECT NO. c. d.	9a ORIGINATOR'S REPORT NUMBER(S) ITR-1/F33 9b OTHER REPORT NO(S) (Any other numbers that may be assigned this report)

10 AVAILABILITY/LIMITATION NOTICES

Qualified requesters may obtain copies of this report from DDC.

11 SUPPLEMENTARY NOTES	12 SPONSORING MILITARY ACTIVITY
	Air Force Avionics Laboratory Division Research and Technology Air Force Systems Command Wright-Patterson Air Force Base, Ohio.

13 ABSTRACT

The general objectives of this contract are to extend the lifetime and reliability of high power ion lasers and to improve their operating characteristics. Specific tasks which will be undertaken during the program are outlined. A cathode evaluation program has been initiated; complete life test data on a hot oxide cathode are presented. The results of an evaluation of pyrolytic graphite and pyrolytic overcoated graphite segments are given. An improved design of radiation-coded anode has been developed and tested. Preliminary studies of noise modulation of the output beam with particular emphasis on fluctuations introduced by power supply ripple are described.

63

DD FORM 1 JAN 64 1473

Unclassified

Security Classification

14 KEY WORDS	LINK A		LINK B		LINK C	
	ROLE	WT	ROLE	WT	ROLE	WT
Argon Ion Laser Ion Laser Gas Laser						

INSTRUCTIONS

1. ORIGINATING ACTIVITY: Enter the name and address of the contractor, subcontractor, grantee, Department of Defense activity or other organization *(corporate author)* issuing the report.

2a. REPORT SECURITY CLASSIFICATION: Enter the overall security classification of the report. Indicate whether "Restricted Data" is included. Marking is to be in accordance with appropriate security regulations.

2b. GROUP: Automatic downgrading is specified in DoD Directive 5200.10 and Armed Forces Industrial Manual. Enter the group number. Also, when applicable, show that optional markings have been used for Group 3 and Group 4 as authorized.

3. REPORT TITLE: Enter the complete report title in all capital letters. Titles in all cases should be unclassified. If a meaningful title cannot be selected without classification, show title classification in all capitals in parenthesis immediately following the title.

4. DESCRIPTIVE NOTES: If appropriate, enter the type of report, e.g., interim, progress, summary, annual, or final. Give the inclusive dates when a specific reporting period is covered.

5. AUTHOR(S): Enter the name(s) of author(s) as shown on or in the report. Enter last name, first name, middle initial. If military, show rank and branch of service. The name of the principal author is an absolute minimum requirement.

6. REPORT DATE: Enter the date of the report as day, month, year; or month, year. If more than one date appears on the report, use date of publication.

7a. TOTAL NUMBER OF PAGES: The total page count should follow normal pagination procedures, i.e., enter the number of pages containing information.

7b. NUMBER OF REFERENCES: Enter the total number of references cited in the report.

8a. CONTRACT OR GRANT NUMBER: If appropriate, enter the applicable number of the contract or grant under which the report was written.

8b, 8c, & 8d. PROJECT NUMBER: Enter the appropriate military department identification, such as project number, subproject number, system numbers, task number, etc.

9a. ORIGINATOR'S REPORT NUMBER(S): Enter the official report number by which the document will be identified and controlled by the originating activity. This number must be unique to this report.

9b. OTHER REPORT NUMBER(S): If the report has been assigned any other report numbers *(either by the originator or by the sponsor)*, also enter this number(s).

10. AVAILABILITY/LIMITATION NOTICES: Enter any limitations on further dissemination of the report, other than those imposed by security classification, using standard statements such as:

(1) "Qualified requesters may obtain copies of this report from DDC."

(2) "Foreign announcement and dissemination of this report by DDC is not authorized."

(3) "U. S. Government agencies may obtain copies of this report directly from DDC. Other qualified DDC users shall request through

_____."

(4) "U. S. military agencies may obtain copies of this report directly from DDC. Other qualified users shall request through

_____."

(5) "All distribution of this report is controlled. Qualified DDC users shall request through

_____."

If the report has been furnished to the Office of Technical Services, Department of Commerce, for sale to the public, indicate this fact and enter the price, if known.

11. SUPPLEMENTARY NOTES: Use for additional explanatory notes.

12. SPONSORING MILITARY ACTIVITY: Enter the name of the departmental project office or laboratory sponsoring *(paying for)* the research and development. Include address.

13. ABSTRACT: Enter an abstract giving a brief and factual summary of the document indicative of the report, even though it may also appear elsewhere in the body of the technical report. If additional space is required, a continuation sheet shall be attached.

It is highly desirable that the abstract of classified reports be unclassified. Each paragraph of the abstract shall end with an indication of the military security classification of the information in the paragraph, represented as *(TS), (S), (C), or (U)*.

There is no limitation on the length of the abstract. However, the suggested length is from 150 to 225 words.

14. KEY WORDS: Key words are technically meaningful terms or short phrases that characterize a report and may be used as index entries for cataloging the report. Key words must be selected so that no security classification is required. Identifiers, such as equipment model designation, trade name, military project code name, geographic location, may be used as key words but will be followed by an indication of technical context. The assignment of links, rules, and weights is optional.